


Spin-orbital model for fullerides

Ryuta Iwazaki  and Shintaro Hoshino

Department of Physics, Saitama University, Shimo-Okubo, Saitama 338-8570, Japan



(Received 8 March 2021; revised 24 May 2021; accepted 1 June 2021; published 21 June 2021)

The multiorbital Hubbard model in the strong-coupling limit is analyzed for the effectively antiferromagnetic Hund's coupling relevant to fulleride superconductors with three orbitals per molecule. The localized spin-orbital model describes the thermodynamics of the half-filled (three electron) state with total spin $1/2$, composed of a singlon and a doublon placed on two of the three orbitals. The model is solved using the mean-field approximation, and magnetic and electric ordered states are clarified through the temperature dependences of the order parameters. Combining the model with the band structure from *ab initio* calculation, we also semiquantitatively analyze the realistic model and the corresponding physical quantities. In the A15-structure fulleride model, there is an antiferromagnetic ordered state, and subsequently the two-orbital ordered state appears at lower temperatures. It is argued that the origin of these orbital orders is related to the T_h point-group symmetry. As for the fcc fulleride model, a time-reversal-broken orbital ordered state is identified. Whereas the spin degeneracy remains in our treatment for a geometrically frustrated lattice, it is expected to be lifted by some magnetic ordering or quantum fluctuations, but not by the spin-orbital coupling, which is effectively zero for fullerides in the strong-coupling regime.

DOI: [10.1103/PhysRevB.103.235145](https://doi.org/10.1103/PhysRevB.103.235145)

I. INTRODUCTION

Strongly correlated electron systems with multiple orbital degrees of freedom show a variety of intriguing phenomena and are realized in a wide range of materials such as iron pnictides, heavy-electron materials, and molecular-based organic materials. The alkali-doped fullerides are also the typical cases where the strong correlation effects with multiorbitals are relevant. This material has been attracting attention in recent years for a lot of experimental findings. The superconductivity with the high transition temperature ~ 40 K is one of the characteristic features [1–8]. While the mechanism is identified as the electron-phonon interaction [9–11], the superconducting dome in the temperature-pressure phase diagram is found to be located near the Mott insulator and antiferromagnetic phase, featuring the typical behaviors of strongly correlated superconductors [7,12–14]. In the Mott insulating phase, the localized electrons form a low-spin state, and the imbalance of the occupancy in orbitals leads to the deformation of the fullerene molecule because of the coupling between electrons and anisotropic molecular distortions (Jahn-Teller phonon). Interestingly, such behavior can also be seen in the metallic phase near the Mott insulator but is absent far away from it [15,16]. This anomalous behavior is called a Jahn-Teller metal where the multiorbital degrees of freedom play an important role. The fullerides are also crystallized on the substrate, and the characteristic asymmetry between electron and hole doping is identified [17,18]. Furthermore, a possible superconducting state has been discussed under the excitation by light above the transition temperature [19,20]. Thus the fulleride materials have been providing intriguing phenomena up until recently.

The alkali-doped fullerides are systems with triply degenerate t_{1u} molecular orbitals which resemble atomic p electrons in nature. There, although the original Hund's coupling inside the fullerene molecule is slightly ferromagnetic, the anisotropic molecular vibration makes the Hund's coupling effectively antiferromagnetic [10,13,21] and is crucial for the low-temperature physics. This is confirmed also from the first-principles calculation [13,22]. The multiorbital Hubbard model with antiferromagnetic Hund's coupling has been studied theoretically, and the various phase diagrams are clarified using the dynamical mean-field theory (DMFT) suitable for the description of the electronically ordered states [21–29]. The Jahn-Teller metal has been interpreted as a spontaneous orbital selective Mott state [26,30], which is an unconventional type of orbital order. The orbital asymmetric feature has also been reported in two-dimensional fullerides using the many-variable variational Monte Carlo method [31].

With the antiferromagnetic Hund's coupling, one of the intramolecular interactions, pair hopping, plays an important role: It activates the dynamics of the double occupancy in an orbital (doublon). In order to clarify the characters of the existing fulleride materials in detail, we focus our attention on the Mott insulating phase, where the doublon physics can be tackled with reasonable computational cost even in a realistic situation. As is well known, for a single-orbital case, the electronic behaviors in the strong-coupling regime are determined by the Heisenberg model of localized electrons. The extension of the Heisenberg model to the multiorbital system is known as the Kugel-Khomskii model, which has been derived for the ferromagnetic Hund's coupling [32,33] and describes the degrees of freedom of the spin and orbital. The spin-orbital models have been applied to the e_g or t_{2g}

d -orbital system [34–37]. On the other hand, the fullerenes have antiferromagnetic Hund’s coupling, so that their strongly correlated effective model differs from the usual Kugel-Khomskii model. While the localized model with antiferromagnetic Hund’s coupling has been constructed for a density-density-type interaction [28], here we deal with more complicated but realistic situations.

In this paper, we develop the localized spin-orbital model for a system with antiferromagnetic Hund’s coupling. We analyze both the symmetric model and the realistic model for fullerenes; the results of the former are easier to interpret and are useful as a reference. The obtained effective model itself is exact in the strong-coupling limit. We solve the model by using the mean-field theory. Since the intersite correlation is included in the mean-field level in DMFT, our results for the ordered states are the same as those obtained by DMFT in the strong-coupling regime. Our method is much more efficient compared with DMFT in this regime. Hence we can perform thorough calculations with full on-site interactions and the complicated hopping in realistic situations.

For the spherical model on a bipartite lattice, we obtain the staggered magnetic ordered state and also the uniform orbital ordered state at the lower-temperature regime. This orbital ordered state is not characterized by the ordinary orbital moment but by the doublon’s orbital moment. In the A15 fulleride effective model, which is a bipartite lattice, we reveal that there are two kinds of orbital ordered states below the antiferromagnetic transition temperature. The obtained orbital ordered states are interpreted as related to an effective recovery of the fourfold symmetry at low temperatures in the T_h point group. We also analyze the geometrically frustrated fcc fulleride model seeking for a spatially uniform ordered state. We reveal that the fcc model has the time-reversal-symmetry-broken orbital ordered state, where the spin ordered state is absent since the spin-orbit coupling on the fullerene molecule is effectively zero.

This paper is organized as follows. We discuss the construction of strongly correlated effective models and the theoretical method in Sec. II. In Sec. III, we show numerical results for the model with isotropic hopping (spherical model introduced in Sec. III A). Section IV provides numerical results for the spin-orbital model combined with A15 and fcc fulleride band structure. We summarize the results in Sec. V.

II. CONSTRUCTION OF MODELS

A. Three-orbital Hubbard model in the strong-coupling limit

Let us begin with the three-orbital Hubbard model

$$\mathcal{H} = \mathcal{H}_t + \mathcal{H}_U, \quad (1)$$

$$\mathcal{H}_t = - \sum_{i \neq j, \gamma, \gamma', \sigma} t_{ij}^{\gamma\gamma'} c_{i, \gamma, \sigma}^\dagger c_{j, \gamma', \sigma}, \quad (2)$$

$$\begin{aligned} \mathcal{H}_U = & \frac{U}{2} \sum_{i, \gamma, \sigma, \sigma'} c_{i, \gamma, \sigma}^\dagger c_{i, \gamma, \sigma'}^\dagger c_{i, \gamma, \sigma'} c_{i, \gamma, \sigma} \\ & + \frac{U'}{2} \sum_{i, \gamma \neq \gamma', \sigma, \sigma'} c_{i, \gamma, \sigma}^\dagger c_{i, \gamma', \sigma'}^\dagger c_{i, \gamma', \sigma'} c_{i, \gamma, \sigma} \end{aligned}$$

$$\begin{aligned} & + \frac{J}{2} \sum_{i, \gamma \neq \gamma', \sigma, \sigma'} (c_{i, \gamma, \sigma}^\dagger c_{i, \gamma', \sigma'}^\dagger c_{i, \gamma, \sigma'} c_{i, \gamma', \sigma} \\ & + c_{i, \gamma, \sigma}^\dagger c_{i, \gamma, \sigma'}^\dagger c_{i, \gamma', \sigma'} c_{i, \gamma', \sigma}), \end{aligned} \quad (3)$$

where $c_{i, \gamma, \sigma}$ ($c_{i, \gamma, \sigma}^\dagger$) is an annihilation (creation) operator at site i of fullerenes with the t_{1u} molecular orbital index $\gamma = x, y, z$ and spin $\sigma = \uparrow, \downarrow$. We deal with the Hilbert space with a fixed number of electrons. We assume the condition $U' = U - 2J$ for the local interaction part in the following discussion, which is valid for the spherical limit. Indeed, this condition is nearly satisfied in the fullerenes as confirmed numerically [38]. In this paper, we consider a strong-coupling regime ($\mathcal{H}_U \gg \mathcal{H}_t$). When we develop the effective model in this limit, the presence of the Hund’s coupling J makes theoretical treatment complicated since it realizes quantum-mechanically superposed local wave functions. Especially for the negative (antiferromagnetic) J relevant to fullerenes, the pair hopping plays an important role which creates the dynamics of doubly occupied electrons at an orbital (doublon). As shown in the following, in order to diminish the difficulty, we use a symbolic expression without elaborating each intermediate process explicitly.

In order to apply the perturbation theory from the strong-coupling limit, we first consider the ground state of the unperturbed Hamiltonian \mathcal{H}_U . Alkali-doped fullerenes with a half-filled situation (three electrons per t_{1u} orbital) have sixfold degenerate ground states written as

$$|\gamma, \sigma\rangle_i = \frac{1}{\sqrt{2}} c_{i, \gamma, \sigma}^\dagger \sum_{\gamma' \neq \gamma} b_{i, \gamma'}^\dagger |0\rangle, \quad (4)$$

where we have defined an orbital-dependent doublon-creation operator as

$$b_{i, \gamma}^\dagger = c_{i, \gamma, \downarrow}^\dagger c_{i, \gamma, \uparrow}^\dagger. \quad (5)$$

The vacuum has been expressed as $|0\rangle$. These states are uniquely characterized by the spin and orbital of the electron at the singly occupied orbital, which is called a “singlon” to contrast with doublons. A schematic picture of the three-electron state $|\gamma, \sigma = \uparrow\rangle_i$ is given in Fig. 1.

In order to understand the energy level structure for the $n = 3$ case, in Fig. 2, we show the Hund’s coupling dependence of the single-site eigenenergies. The line with blue circles represents the eigenenergy for the spin $S = 3/2$ states, which takes $3U - 9J$. The line with orange triangles corresponds to the spin singlet with bonding doublon states, and their energies are $3U - 4J$. The line with green diamonds shows the eigenenergy $3U - 6J$ for the other types of eigenstates. These lines cross at $J/U = 0$. Since the transition metals have the ferromagnetic Hund’s coupling, the ground state is the high-spin state, which accords with the region $J/U > 0$ in Fig. 2. On the other hand, in the case with $J/U < 0$, which is realized in the fullerenes, the low-spin state is energetically favored, and the ground state is therefore $|\gamma, \sigma\rangle_i$ defined in Eq. (4).

Using the above Hamiltonian, the second-order effective Hamiltonian is written as

$$\mathcal{H}_{\text{eff}} = \mathcal{P} \mathcal{H}_t \frac{1}{-\mathcal{H}_U} \mathcal{Q} \mathcal{H}_t \mathcal{P}, \quad (6)$$

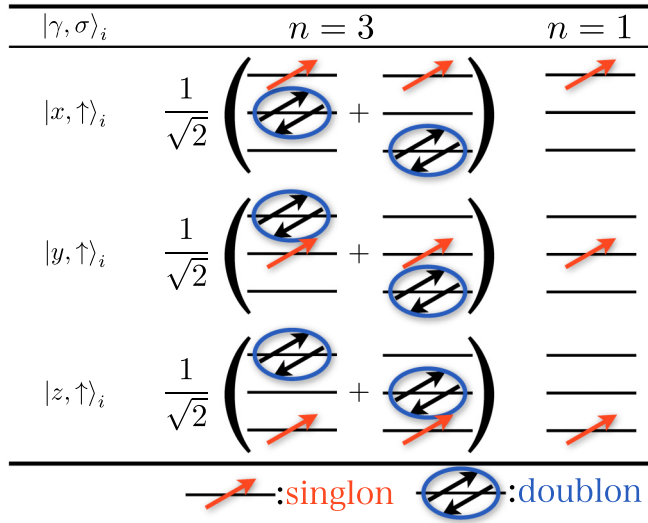


FIG. 1. Schematic pictures of the ground-state wave functions $|\gamma, \sigma = \uparrow\rangle_i$ of the local Hamiltonian for $n = 3$ and $n = 1$.

where \mathcal{P} is a projection operator to a model space described by Eq. (4) as

$$\mathcal{P} = \prod_i \sum_{\gamma, \sigma} |\gamma, \sigma\rangle_i \langle \gamma, \sigma| \quad (7)$$

and $\mathcal{Q} = 1 - \mathcal{P}$. We have used $[\mathcal{P}, \mathcal{H}_U] = 0$. The energy is measured from the ground state of \mathcal{H}_U . The size of our model space is 6^N , where $N = \sum_i 1$ is the number of lattice sites.

The strategy for obtaining the concrete form of the effective Hamiltonian is to consider the two-site problem. We first prepare the $2^{12} \times 2^{12}$ matrix expressions for the annihilation and creation operators for the two-site problem ($12 = \sum_{i, \gamma, \sigma} 1$) and then define all of the matrix expressions given

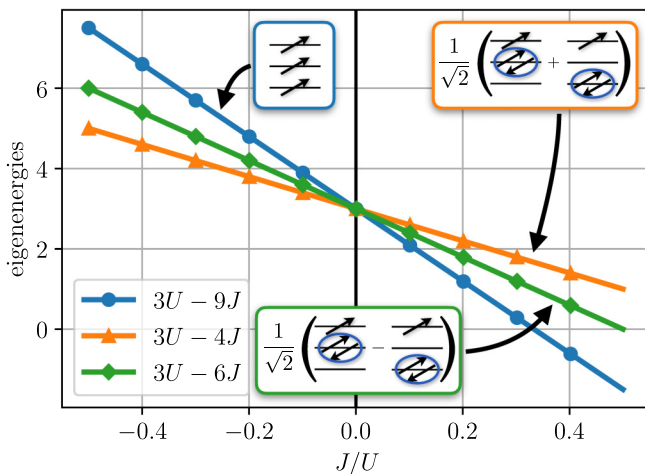


FIG. 2. Hund's coupling dependence of the single-site energies for the $n = 3$ model. The insets are schematic pictures of one of the eigenstates for each energy level. The blue circles and the orange triangles show the energies for the spin $S = 3/2$ states and the spin singlet with bonding doublon states, respectively. The green diamonds show the energy of the other types of eigenstates, which never become a ground state.

in Eq. (6). Performing multiplications of such matrices, we obtain the two-site effective Hamiltonian in the form of the $6^2 \times 6^2$ matrix. We expand the above effective Hamiltonian by following local operators $O_i^{\eta\mu}$ defined as

$$O_i^{\eta\mu} = \sum_{\gamma, \gamma'} \sum_{\sigma, \sigma'} |\gamma, \sigma\rangle_i \lambda_{\gamma\gamma'}^{\eta} \sigma_{\sigma\sigma'}^{\mu} \langle \gamma', \sigma'|, \quad (8)$$

in the model Hilbert space. $\sigma^{\mu=0,x,y,z}$ is the Pauli matrix

$$\begin{aligned} \sigma^0 &= \begin{pmatrix} 1 & 0 \\ 0 & 1 \end{pmatrix}, & \sigma^x &= \begin{pmatrix} 0 & 1 \\ 1 & 0 \end{pmatrix}, \\ \sigma^y &= \begin{pmatrix} 0 & -i \\ i & 0 \end{pmatrix}, & \sigma^z &= \begin{pmatrix} 1 & 0 \\ 0 & -1 \end{pmatrix}, \end{aligned} \quad (9)$$

which represents the degrees of freedom of the spin. Another matrix $\lambda^{\eta=0,\dots,8}$ is given by

$$\begin{aligned} \lambda^0 &= \sqrt{\frac{2}{3}} \begin{pmatrix} 1 & 0 & 0 \\ 0 & 1 & 0 \\ 0 & 0 & 1 \end{pmatrix}, & \lambda^1 &= \begin{pmatrix} 0 & -1 & 0 \\ -1 & 0 & 0 \\ 0 & 0 & 0 \end{pmatrix}, \\ \lambda^2 &= \begin{pmatrix} 0 & -i & 0 \\ i & 0 & 0 \\ 0 & 0 & 0 \end{pmatrix}, & \lambda^3 &= \begin{pmatrix} -1 & 0 & 0 \\ 0 & 1 & 0 \\ 0 & 0 & 0 \end{pmatrix}, \\ \lambda^4 &= \begin{pmatrix} 0 & 0 & -1 \\ 0 & 0 & 0 \\ -1 & 0 & 0 \end{pmatrix}, & \lambda^5 &= \begin{pmatrix} 0 & 0 & i \\ 0 & 0 & 0 \\ -i & 0 & 0 \end{pmatrix}, \\ \lambda^6 &= \begin{pmatrix} 0 & 0 & 0 \\ 0 & 0 & -1 \\ 0 & -1 & 0 \end{pmatrix}, & \lambda^7 &= \begin{pmatrix} 0 & 0 & 0 \\ 0 & 0 & -i \\ 0 & i & 0 \end{pmatrix}, \\ \lambda^8 &= \sqrt{\frac{1}{3}} \begin{pmatrix} 1 & 0 & 0 \\ 0 & 1 & 0 \\ 0 & 0 & -2 \end{pmatrix}; \end{aligned} \quad (10)$$

these matrices are slightly different from the ordinary definition of the Gell-Mann matrices to make them suitable for p -electron systems. We note that the above local operators satisfy the orthonormal relation

$$\text{Tr}[O_i^{\eta\mu} O_j^{\eta'\mu'}] = 4\delta_{ij} \delta^{\eta\eta'} \delta^{\mu\mu'}. \quad (11)$$

Thus the set of operators $O_i^{\eta\mu}$ is regarded as a basis set of the extended Hilbert space (Liouville space). In contrast, the states $|\gamma, \sigma\rangle_i$ are the basis in the six-component model Hilbert space. Extending the two-site problem to the full lattice, we obtain the effective Hamiltonian in the strong-coupling limit

$$\mathcal{H}_{\text{eff}} = \sum_{i,j} \sum_{\eta, \eta'} \sum_{\mu, \mu'} I_{ij}^{\eta\mu; \eta'\mu'} O_i^{\eta\mu} O_j^{\eta'\mu'}. \quad (12)$$

This model is to be analyzed in the rest of this paper. We will show the explicit form of the coupling constant $I_{ij}^{\eta\mu; \eta'\mu'}$ for the case of the spherical model in Secs. III B 1 and III C 1.

We also comment on the orbital moments in the restricted Hilbert space. In terms of the original Hubbard model, the local orbital moment is defined by

$$\mathcal{L}_i \equiv \sum_{\gamma, \gamma', \sigma} c_{i, \gamma, \sigma}^\dagger \ell_{\gamma\gamma'} c_{i, \gamma', \sigma}, \quad (13)$$

where the 3×3 matrices are given by $\ell_x = \lambda^7$, $\ell_y = \lambda^5$, and $\ell_z = \lambda^2$. This angular momentum operator is, however, zero for the restricted Hilbert space:

$$\mathcal{P}\mathcal{L}_i\mathcal{P} = \mathbf{0}. \quad (14)$$

This anomalous disappearance of the angular momentum is due to the composite nature of the ground state [26] and is very different from a singly occupied state. Then the active orbital degrees of freedom are not of the original electrons but of the three-electron composite involving doublons. This feature also affects the spin-orbit coupling, which takes the form

$$\mathcal{H}_{\text{SO}} = \frac{1}{2}\lambda_{\text{SO}} \sum_i \sum_{\gamma, \gamma'} \sum_{\sigma, \sigma'} c_{i, \gamma, \sigma}^\dagger \boldsymbol{\ell}_{\gamma\gamma'} \cdot \boldsymbol{\sigma}_{\sigma\sigma'} c_{i, \gamma', \sigma'}, \quad (15)$$

in the language of the original multiorbital Hubbard model. The spin-orbit coupling for a $2p$ electron in a carbon atom is nearly 2 meV, and because of the extended nature of the fullerene molecule the spin-orbit coupling λ_{SO} for t_{1u} orbitals is 100 times smaller than the atomic value ($\lambda_{\text{SO}} \sim 20 \mu\text{eV}$) [39]. Furthermore, for the restricted Hilbert space of $n = 3$ states, the effect of the spin-orbit coupling enters only through the second-order perturbation contribution as

$$\begin{aligned} \mathcal{H}_{\text{SO}}^{(2)} &= \mathcal{P}\mathcal{H}_{\text{SO}} \frac{1}{-\mathcal{H}_U} \mathcal{Q}\mathcal{H}_{\text{SO}}\mathcal{P} \\ &= \frac{1}{2}\Lambda_{\text{SO}} \sum_i \sum_{\gamma, \gamma'} \sum_{\sigma, \sigma'} |\gamma, \sigma\rangle_i \boldsymbol{\ell}_{\gamma\gamma'} \cdot \boldsymbol{\sigma}_{\sigma\sigma'} |\gamma', \sigma'\rangle_i, \end{aligned} \quad (16)$$

where $\Lambda_{\text{SO}} = \frac{11\lambda_{\text{SO}}^2}{20J}$ for $J < 0$. Using the value for the antiferromagnetic coupling $J \sim -0.03 \text{ eV}$ for fullerenes [38], we obtain $\Lambda_{\text{SO}} \sim 1 \text{ neV}$, which is tiny. Hence we can safely neglect the spin-orbit coupling in fullerenes.

It is convenient to recognize that the above three-electron state is similar to the singly occupied state

$$|n = 1, \gamma, \sigma\rangle_i = c_{i, \gamma, \sigma}^\dagger |0\rangle, \quad (18)$$

which is the eigenstate with $n_i = \sum_{\gamma, \sigma} c_{i, \gamma, \sigma}^\dagger c_{i, \gamma, \sigma} = 1$ regardless of the sign of J (see the right column of Fig. 1). In this paper, the number of electrons is fixed at each site, and n_i is sometimes simply written as n . In Eq. (18), we explicitly write “ $n = 1$,” and if it is dropped, the state represents the $n = 3$ state defined in Eq. (4). The ground state for $n = 3$ is obtained by filling the empty orbital in the $n = 1$ state with the doublons as in Eq. (4).

We will consider the $n = 1$ case for reference to illuminate the characteristics of $n = 3$ relevant to fullerenes. When we deal with the second-order effective Hamiltonian for the $n = 1$ states, we just replace $|\gamma, \sigma\rangle_i$ with $|n = 1, \gamma, \sigma\rangle_i$ defined in Eq. (18). We note that, in this case, the angular momentum does not vanish as distinct from the $n = 3$ multiplet. For the usual ferromagnetic Hund’s coupling ($J > 0$), the system corresponds to the spin-orbital model considered for the t_{2g} orbitals of d electrons [37].

B. Mean-field approximations

In this paper, we utilize the mean-field approximation (MFA) for the obtained effective Hamiltonian. We apply the

external field for convenience, and the full Hamiltonian is written as

$$\mathcal{H}_{\text{eff}} = \frac{1}{2} \sum_{i,j} \vec{O}_i^\dagger \hat{t}_{ij} \vec{O}_j - \sum_i \vec{H}_i^\dagger \vec{O}_i \quad (19)$$

$$\begin{aligned} &\approx - \sum_{i,j} \left[\vec{H}_i^\dagger \delta_{ij} \hat{1} - \frac{1}{2} \vec{\mathcal{M}}_i^\dagger (\hat{t}_{ij} + \hat{t}_{ji}^\dagger) \right] \vec{O}_j \\ &- \frac{1}{2} \sum_{i,j} \vec{\mathcal{M}}_i^\dagger \hat{t}_{ij} \vec{\mathcal{M}}_j \equiv \mathcal{H}^{\text{MF}}, \end{aligned} \quad (20)$$

where the hat and arrow symbols represent the matrix and vector, respectively, with respect to the intrasite degrees of freedom (η, μ). The vector \vec{O}_i is the operator for the order parameter at site i , whose matrix representation is given in Eq. (8). Namely, it is a column vector having 35 components, each of which is a 6×6 matrix where the identity is eliminated. The statistical average $\vec{\mathcal{M}}_i = \langle \vec{O}_i \rangle$ is the order parameter. In this paper, the coupling constant \hat{t}_{ij} connects only nearest-neighbor (NN) sites for the spherical model (Sec. III) and NN and next-nearest-neighbor (NNN) sites for the A15 and fcc fullerene models (Sec. IV). In the rest of this section, we concentrate on the bipartite lattice, such as the A15 structure. Then we introduce two kinds of AB sublattice to describe staggered orders. For a nonbipartite lattice (i.e., fcc), on the other hand, we consider only the uniform solution, and a similar formula can easily be obtained by regarding the two sublattices as identical.

The mean-field Hamiltonian is then rewritten as

$$\begin{aligned} \mathcal{H}^{\text{MF}} &= - \sum_\alpha \left[\vec{H}_\alpha^\dagger - \frac{1}{2} \sum_{\delta \in \text{NN}} \vec{\mathcal{M}}_\alpha^\dagger (\hat{t}_{\delta,0} + \hat{t}_{0,\delta}^\dagger) \right. \\ &\quad \left. - \frac{1}{2} \sum_{\delta \in \text{NNN}} \vec{\mathcal{M}}_\alpha^\dagger (\hat{t}_{\delta,0} + \hat{t}_{0,\delta}^\dagger) \right] \sum_{i \in \alpha} \vec{O}_i \\ &\quad - \frac{1}{2} \frac{N}{2} \sum_\alpha \left[\sum_{\delta \in \text{NN}} \vec{\mathcal{M}}_\alpha^\dagger \hat{t}_{\delta,0} \vec{\mathcal{M}}_\alpha + \sum_{\delta \in \text{NNN}} \vec{\mathcal{M}}_\alpha^\dagger \hat{t}_{\delta,0} \vec{\mathcal{M}}_\alpha \right], \end{aligned} \quad (21)$$

where $\alpha = \text{A, B}$ is the sublattice index and $\bar{\alpha}$ is a complementary component of α , i.e., $\bar{\text{A}} = \text{B}$ and $\bar{\text{B}} = \text{A}$. N is the number of sites. The number of $\delta \in \text{NN}$ is z , 8, or 12 for the spherical, A15, or fcc model, respectively. As for $\delta \in \text{NNN}$, both the A15 case and the fcc case have six sites. We have used the fact that the NN-connected sites belong to different sublattices and the NNN-connected sites belong to the same sublattice. Since the coupling constants are dependent only on the direction of the vector connecting two sites, we write the interaction parameter as $\hat{t}_{\delta,0}$, where the index 0 represents the site which we focus on.

For the bipartite lattice, we introduce the uniform and staggered moments as

$$\begin{pmatrix} \vec{\mathcal{M}}_{\text{u}} \\ \vec{\mathcal{M}}_{\text{s}} \end{pmatrix} = \frac{1}{\sqrt{2}} \begin{pmatrix} \hat{1} & \hat{1} \\ \hat{1} & -\hat{1} \end{pmatrix} \begin{pmatrix} \vec{\mathcal{M}}_{\text{A}} \\ \vec{\mathcal{M}}_{\text{B}} \end{pmatrix}. \quad (22)$$

This expression is useful in analyzing the mean-field solutions shown later.

Now we explain the method of numerical calculation. The solutions are obtained by renewing the order parameters iteratively using the self-consistent equation. The free energy and the self-consistent equation are given by

$$\mathcal{F} = -T \ln Z, \quad (23)$$

$$\vec{\mathcal{M}}_\alpha = -\frac{\partial \mathcal{F}}{\partial \vec{H}_\alpha}, \quad (24)$$

where $Z = \text{Tr} e^{-\beta \mathcal{H}_{\text{MF}}}$ is the partition function made of the mean-field Hamiltonian. For the derivation of the self-consistent equation, the parameters \vec{H} and $\vec{\mathcal{M}}$ must be regarded as independent variables.

The system with the present effective Hamiltonian has 35 kinds of order parameters per site, and there may exist several solutions which take the same free energy as they are connected by symmetries. In the next sections, we show the simplest form of the order parameters among those energetically degenerate solutions.

C. Response functions

In this subsection, we consider the response function to the weak static field. We expand the mean-field Hamiltonian up to first order of the field

$$\mathcal{H}^{\text{MF}} = \mathcal{H}^{(0)} + \mathcal{H}^{(1)} + \mathcal{O}(H^2), \quad (25)$$

$$\mathcal{H}^{(0)} = \sum_{i,j} (\vec{\mathcal{M}}_i^{(0)})^T \hat{t}_{ij} \vec{\mathcal{O}}_j, \quad (26)$$

$$\mathcal{H}^{(1)} = - \sum_{i,j} \left[\vec{H}_i^T \delta_{ij} - (\vec{\mathcal{M}}_i^{(1)})^T \hat{t}_{ij} \right] \vec{\mathcal{O}}_j, \quad (27)$$

where the superscript represents the perturbative order of the field and we have neglected the constant term. When we define the effective field as $\vec{\tilde{H}}_i = \vec{H}_i - \sum_j \hat{t}_{ji}^T \vec{\mathcal{M}}_j^{(1)}$ and treat $\mathcal{H}^{(1)}$ as the perturbation, we obtain the following linear response relation:

$$\vec{\mathcal{M}}_i^{(1)} = \sum_j \hat{\chi}_{ij}^{(0)} \vec{\tilde{H}}_j = \sum_j \hat{\chi}_{ij} \vec{H}_j, \quad (28)$$

where $\hat{\chi}$ is the full susceptibility for the bare external field \vec{H}_i . According to linear response theory, the zeroth-order susceptibility is obtained by

$$\hat{\chi}_{ij}^{(0)} = \int_0^{1/T} d\tau \left[\langle T_\tau \vec{\mathcal{O}}_i \vec{\mathcal{O}}_j^T(\tau) \rangle_0 - \vec{\mathcal{M}}_i^{(0)} (\vec{\mathcal{M}}_j^{(0)})^T \right], \quad (29)$$

where τ is an imaginary time and T_τ is the imaginary time ordering operator. The Heisenberg picture at an imaginary time is expressed as

$$\vec{\mathcal{O}}_i(\tau) = e^{\tau \mathcal{H}^{(0)}} \vec{\mathcal{O}}_i e^{-\tau \mathcal{H}^{(0)}}. \quad (30)$$

$\langle \cdots \rangle_0$ represents the statistical average with $\mathcal{H}^{(0)}$. The susceptibility matrix $\hat{\chi}_{ij}^{(0)}$ has only the intrasite component since each site is independent under the MFA. Substituting the concrete expression into the effective field in Eq. (28), we obtain

$$\sum_j \left[\delta_{ij} \hat{1} + \sum_k \hat{\chi}_{ik}^{(0)} \hat{t}_{kj}^T \right] \vec{\mathcal{M}}_j^{(1)} = \sum_j \hat{\chi}_{ij}^{(0)} \vec{H}_j. \quad (31)$$

Then, taking the matrix inverse of the left-hand side and combining it with Eq. (28), we obtain the susceptibility matrix $\hat{\chi}_{ij}$. For a bipartite lattice, we introduce the uniform and staggered susceptibilities by

$$\hat{\chi}_u = \frac{1}{N} \sum_{i,j} \hat{\chi}_{ij}, \quad (32)$$

$$\hat{\chi}_s = \frac{1}{N} \sum_{i,j} s_i s_j \hat{\chi}_{ij}, \quad (33)$$

where $s_i = +1$ for $i \in A$ and $s_i = -1$ for $i \in B$. This quantity will be shown in the next section. Although we focus on the static response functions in this paper, the above argument can easily be generalized to the dynamical susceptibility, which captures the magnetic and electric dynamics of the localized model.

From the viewpoint of Landau theory, we can also discuss the stability of the solution based on the susceptibilities. We write down the Landau free energy with an order parameter up to second order as

$$\mathcal{F}_L = \frac{1}{2} \sum_{i,j} \vec{\mathcal{M}}_i^T \hat{a}_{ij} \vec{\mathcal{M}}_j - \sum_i \vec{H}_i^T \vec{\mathcal{M}}_i, \quad (34)$$

where \hat{a}_{ij} is a coefficient of the quadratic term. Note that, here, $\vec{\mathcal{M}}$ is defined as the deviation from its equilibrium point. Then we obtain the following equation of states:

$$\sum_j \hat{a}_{ij} \vec{\mathcal{M}}_j = \vec{H}_i. \quad (35)$$

Comparing the linear response function, we find that the Hessian matrix is identical to the inverse susceptibility:

$$\frac{\partial^2 \mathcal{F}_L}{\partial \vec{\mathcal{M}}_i \partial \vec{\mathcal{M}}_j} = \hat{a}_{ij} = (\hat{\chi}^{-1})_{ij}. \quad (36)$$

We can consider the necessary and sufficient condition for the stable solution. Let ε_n be the n th eigenvalue of the matrix \hat{a}_{ij} . Each energy corresponds to the eigenenergy of the excitation modes. We must have the condition

$$\varepsilon_n \geq 0, \quad (37)$$

for all n , if the system is thermodynamically stable. If $\varepsilon_n = 0$ is obtained, it indicates the presence of the Nambu-Goldstone mode. With the use of Eq. (36), in the actual calculations, we obtain ε_n by diagonalizing the inverse susceptibility matrix.

III. NUMERICAL RESULTS FOR SPHERICAL MODELS

In the rest of this paper, we will encounter the successive phase transitions with decreasing temperature. There, we denote each transition temperature as $T_{c1} > T_{c2} > \cdots$. If only one transition temperature is identified, we use T_c to denote it. Note that we use the same symbol for the transition temperatures in different models.

A. Spherical spin-orbital model

First we consider the model in the spherical limit. Namely, we assume the hopping matrix given in Eq. (2) to be

$$\hat{t}_{ij} = \begin{pmatrix} t & 0 & 0 \\ 0 & t & 0 \\ 0 & 0 & t \end{pmatrix}, \quad (38)$$

for a bipartite lattice with coordination number z . Using the spin-orbital operator $O_i^{\eta\mu}$ defined in the previous section, we obtain the spherical model as

$$\begin{aligned} \mathcal{H}_{\text{eff}} = & - \sum_{\langle ij \rangle} \left[I_S \mathbf{S}_i \cdot \mathbf{S}_j + I_L \mathbf{L}_i \cdot \mathbf{L}_j + I_Q \sum_{\eta} Q_i^{\eta} Q_j^{\eta} \right. \\ & \left. + I_R \sum_{\mu} \sum_{\nu} R_i^{\nu,\mu} R_j^{\nu,\mu} + I_T \sum_{\mu} \sum_{\eta} T_i^{\eta,\mu} T_j^{\eta,\mu} + I_0 \right], \end{aligned} \quad (39)$$

where the sum with $\langle ij \rangle$ is taken over the pairs of the NN sites. The superscript μ, ν ($= x, y, z$) and η ($= x^2 - y^2, z^2, xy, yz, zx$) are the indices for the polynomials, which represent the component of the spin, rank 1 orbital, and rank 2 orbital, respectively. We have rewritten the operators in accordance with their symmetries as

$$S_i^{\mu} = \frac{1}{2} O_i^{0\mu}, \quad (40)$$

$$L_i^x = \frac{1}{2} O_i^{70}, \quad L_i^y = \frac{1}{2} O_i^{50}, \quad L_i^z = \frac{1}{2} O_i^{20}, \quad (41)$$

$$\begin{aligned} Q_i^{x^2-y^2} &= \frac{1}{2} O_i^{30}, \quad Q_i^{z^2} = \frac{1}{2} O_i^{80}, \\ Q_i^{xy} &= \frac{1}{2} O_i^{10}, \quad Q_i^{yz} = \frac{1}{2} O_i^{60}, \quad Q_i^{zx} = \frac{1}{2} O_i^{40}, \end{aligned} \quad (42)$$

$$R_i^{x,\mu} = \frac{1}{2} O_i^{7\mu}, \quad R_i^{y,\mu} = \frac{1}{2} O_i^{5\mu}, \quad R_i^{z,\mu} = \frac{1}{2} O_i^{2\mu}, \quad (43)$$

$$\begin{aligned} T_i^{x^2-y^2,\mu} &= \frac{1}{2} O_i^{3\mu}, \quad T_i^{z^2,\mu} = \frac{1}{2} O_i^{8\mu}, \\ T_i^{xy,\mu} &= \frac{1}{2} O_i^{1\mu}, \quad T_i^{yz,\mu} = \frac{1}{2} O_i^{6\mu}, \quad T_i^{zx,\mu} = \frac{1}{2} O_i^{4\mu}. \end{aligned} \quad (44)$$

The physical meaning of each order parameter now becomes clearer with this notation. We call S_i^{μ} a magnetic spin (MS or S), L_i^{μ} a magnetic orbital (MO or L), Q_i^{μ} an electric orbital (EO or Q), $R_i^{\nu,\mu}$ an electric spin-orbital (ESO or R), and $T_i^{\eta,\mu}$ a magnetic spin-orbital (MSO or T) moment. I_0 represents energy gain by the second-order perturbation process. Obviously, Eq. (39) satisfies $\text{SU}(2) \times \text{SO}(3)$ symmetry in spin-orbital space.

We will show the numerical results of the $n = 1$ and $n = 3$ spherical models under the MFA, both of which have the six states per site in the model space as discussed in Sec. II A. We beforehand introduce the following notation with regard to the coupling constants defined in Eq. (39):

$$I_{\xi} = - \sum_n A_{\xi n} \frac{t^2}{\Delta E_n}, \quad (45)$$

for $\xi = S, L, Q, R, T, 0$, where ΔE_n represents all possible excitation energies. Its energy corresponds to the denominator of Eq. (6). The coefficient A is summarized in Tables I and II (see Secs. III B and III C).

Before we show the mean-field results, we discuss the ground-state wave function for the two-site problem. Using

TABLE I. Coefficients A defined in Eq. (45) for the $n = 1$ spherical model. The ground-state energy is zero. We add the details for the intermediate state in the main text. We also list the number of the degeneracy of the excited two-site states.

	ΔE_n		
	$U - 3J$	$U - J$	$U + 2J$
Degeneracy	18	10	2
$\xi = S$	-2	10/3	2/3
$\xi = L$	3	-5/3	2/3
$\xi = Q$	3	-1/3	-2/3
$\xi = R$	1	5/3	-2/3
$\xi = T$	1	1/3	2/3
$\xi = 0$	-6	-10/3	-2/3

the single-site state defined in Eq. (4) or (18), we obtain the two-site (i.e., sites at i and j) ground state as

$$|\text{gs}\rangle = \sum_{\gamma_i, \sigma_i} \sum_{\gamma_j, \sigma_j} C_{\gamma_i \sigma_i, \gamma_j \sigma_j} |\gamma_i, \sigma_i\rangle_i |\gamma_j, \sigma_j\rangle_j. \quad (46)$$

The explicit form of the matrix C is written as

$$\hat{C} = \lambda^0 \otimes (-i\sigma^y). \quad (47)$$

This shows that the ground-state wave function is spin singlet and symmetric on the orbital. This is valid for all the spherical cases considered in this section. For an infinite lattice, as in the single-orbital Hubbard model, the intersite spin singlet state may favor the antiferromagnetic state in the ground state for a bipartite lattice.

B. $n = 1$ model

First of all, we consider the results for the $n = 1$ model. Although the results are not relevant to the alkali-doped fullerenes, this knowledge is useful in interpreting the more complicated model for the spherical $n = 3$ model (Sec. III C) and the realistic A15- (Sec. IV A) and fcc-structure fullerenes (Sec. IV B).

1. Coupling constant

We begin with the analysis of the intermediate states relevant to the second-order perturbation theory. We show the coefficients A defined in Eq. (45) in Table I. We have the three kinds of excited states, whose energy is determined by the local Coulomb interaction. For $\Delta E_n = U - 3J$, the intermediate states are ninefold degenerate spin triplet states, as expressed, e.g., by $c_{i,y,\uparrow}^{\dagger} c_{i,x,\uparrow}^{\dagger} |0\rangle$ and $\frac{1}{\sqrt{2}}(c_{i,y,\downarrow}^{\dagger} c_{i,x,\uparrow}^{\dagger} + c_{i,y,\uparrow}^{\dagger} c_{i,x,\downarrow}^{\dagger}) |0\rangle$. For $\Delta E_n = U - J$, the intermediate states are the interorbital spin singlet states, such as $\frac{1}{\sqrt{2}}(c_{i,y,\downarrow}^{\dagger} c_{i,x,\uparrow}^{\dagger} - c_{i,y,\uparrow}^{\dagger} c_{i,x,\downarrow}^{\dagger}) |0\rangle$, and the intraorbital spin singlet states with antibonding orbitals written as $\frac{\sqrt{2}}{3}(2b_{i,z}^{\dagger} - b_{i,x}^{\dagger} - b_{i,y}^{\dagger}) |0\rangle$. These two kinds of states take the same energy since there is the spherically symmetric condition $U' = U - 2J$. For $\Delta E_n = U + 2J$, there is only one intermediate state, which is the intraorbital spin singlet and bonding state written as $\frac{1}{\sqrt{3}}(b_{i,x}^{\dagger} + b_{i,y}^{\dagger} + b_{i,z}^{\dagger}) |0\rangle$. For example, we can obtain the spin coupling

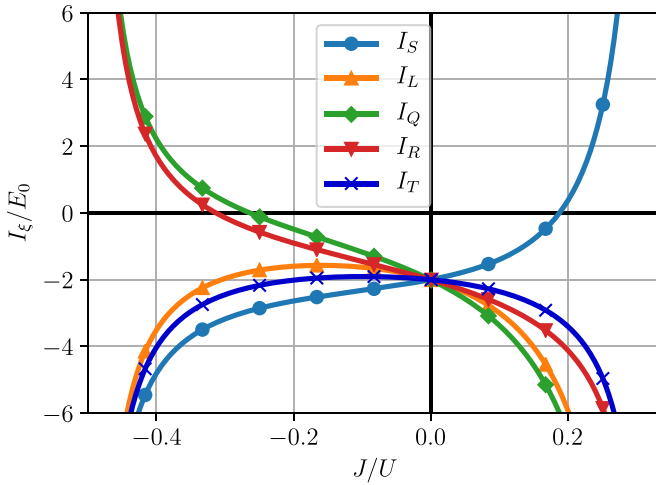


FIG. 3. Hund's coupling ratio J/U dependence of the coupling constants for the $n = 1$ spherical model. The vertical axis is normalized by $E_0 = t^2/U$.

I_S by combining Eq. (45) with Table I as

$$I_S = -\frac{-2t^2}{U-3J} - \frac{\frac{10}{3}t^2}{U-J} - \frac{\frac{2}{3}t^2}{U+2J}. \quad (48)$$

In Table I, we also show the number of the degeneracy of the excited states. We show the Hund's coupling dependence of the coupling constants in Fig. 3. The perturbation theory is justified for $-1/2 < J/U < 1/3$ where the ground states are written in the form of Eq. (18). Taking $J = 0$, the coupling constants become identical. This reflects that the system has $SU(6)$ symmetry and the degrees of freedom of the spin and orbital are equivalent in the absence of Hund's coupling. The largest coupling constant is $|I_S|$ for the antiferromagnetic case ($J < 0$) and $|I_Q|$ for the ferromagnetic Hund's coupling ($J > 0$). This shows that the system tends to have antiferromagnetic (AFM) or antiferro-orbital (AFO) order depending on the sign of the Hund's coupling. This is understood from the intermediate state.

In the case of $J > 0$, which is relevant to the usual t_{2g} -orbital d -electron systems with $n = 1$ per atom, the energetically favorable intermediate two-electron state is interorbital spin triplet. To realize this intermediate state, the initial state needs to occupy a parallel spin configuration with different orbitals such as $c_{i,x,\uparrow}^\dagger c_{j,y,\uparrow}^\dagger |0\rangle$. Therefore the orbital order should be dominant for $J > 0$ as a leading-order ordering instability. If we take $J/U \gtrsim 0.2$, I_S takes a ferromagnetic coupling constant, which favors parallel spins at two sites.

As for $J < 0$, on the other hand, the intermediate state tends to be an intraorbital spin singlet and bonding state. The corresponding initial state must be antiparallel spin with the same orbital such as $c_{i,x,\uparrow}^\dagger c_{j,x,\downarrow}^\dagger |0\rangle$. Thus the magnetic order should be dominant for $J < 0$.

2. Mean-field solutions for antiferromagnetic Hund's coupling ($J < 0$)

Let us turn our attention to the numerical results using the MFA in the spherical model. We take the NN coordination number $z = 6$ in the numerical calculation by assuming

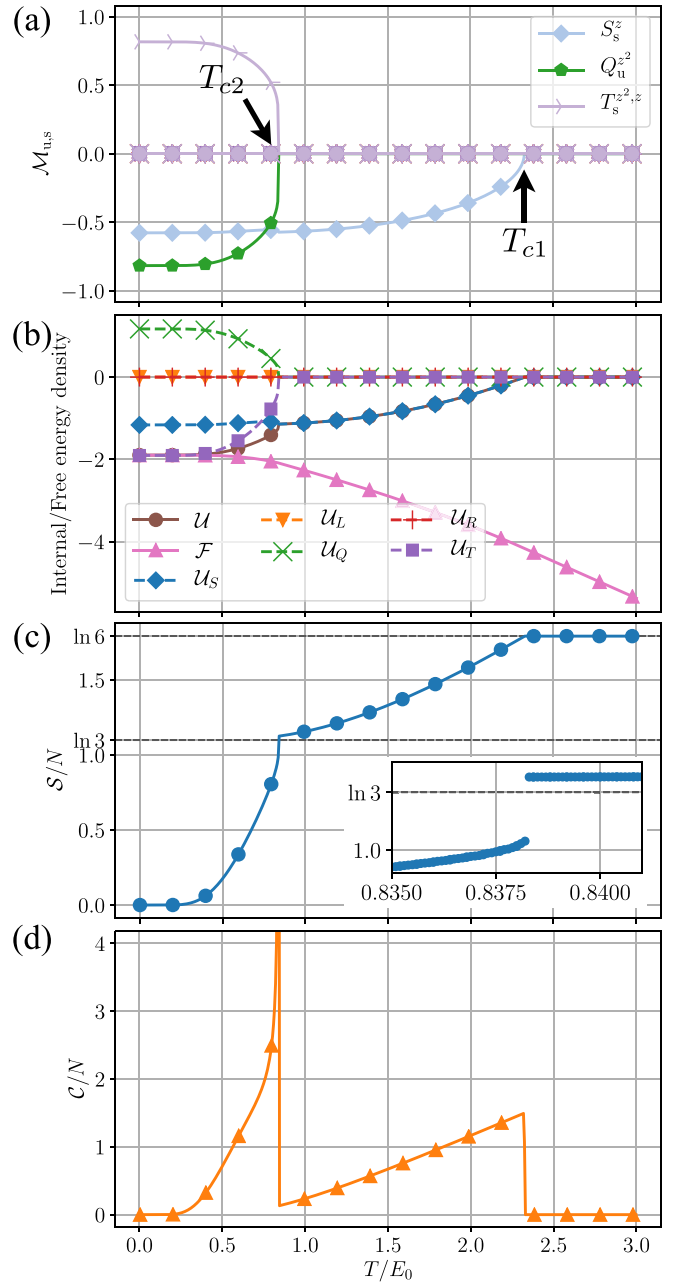


FIG. 4. Temperature dependence of (a) the order parameter, (b) the decomposed internal energy and total free energy density, (c) the entropy, and (d) the specific heat for the $n = 1$, $J/U = -0.1$ bipartite spherical model. The inset in (c) is an enlarged plot around T_{c2} . The energy unit of these plots is $E_0 = t^2/U$.

a simple cubic lattice in three dimensions. Figure 4 shows the temperature dependence of the physical quantities in the bipartite lattice model at $J/U = -0.1$ (antiferromagnetic Hund's coupling). We take $E_0 \equiv t^2/U$ as the unit of energy. The uniform and staggered order parameters are shown in Fig. 4(a), where the antiferromagnetic spin (AF-S) order appears first with decreasing temperature from the high-temperature limit. This corresponds to the largest coupling constant $|I_S|$ in Fig. 3. At lower temperatures, the ferro (F)-orbital Q moment of z^2 type appears together with the AF-T

(MSO) moments. In order to clarify which is the primary order parameter of the second phase transition at T_{c2} , we show in Fig. 4(b) the internal energy and free energy per site, where the internal energy is decomposed into each contribution as

$$\mathcal{U}_S = I_S \langle \mathbf{S}_A \rangle \cdot \langle \mathbf{S}_B \rangle, \quad (49)$$

$$\mathcal{U}_L = I_L \langle \mathbf{L}_A \rangle \cdot \langle \mathbf{L}_B \rangle, \quad (50)$$

$$\mathcal{U}_Q = I_Q \sum_{\eta} \langle Q_A^{\eta} \rangle \langle Q_B^{\eta} \rangle, \quad (51)$$

$$\mathcal{U}_R = I_R \sum_{\mu} \sum_{\nu} \langle R_A^{\nu, \mu} \rangle \langle R_B^{\nu, \mu} \rangle, \quad (52)$$

$$\mathcal{U}_T = I_T \sum_{\mu} \sum_{\eta} \langle T_A^{\eta, \mu} \rangle \langle T_B^{\eta, \mu} \rangle. \quad (53)$$

The total internal energy is given by $\mathcal{U} = \sum_{\xi} \mathcal{U}_{\xi}$ for $\xi = S, L, Q, R, T$, where the energy is measured from I_0 . We see from Fig. 4(b) that the energy \mathcal{U}_T is gained below T_{c2} but \mathcal{U}_Q is not. Hence the AF- T should be the primary order parameter, and F- Q is just induced by the combination of AF- S plus AF- T moments. The results are consistent with the magnitude relation $|I_T| > |I_Q|$ seen in Fig. 3, where the energy gain obtained from the T moment is larger than the energy loss from Q .

Figure 4(c) shows the temperature dependence of the entropy, where all the entropy is released in the ground state. With increasing temperature, the entropy shows a kink at $T/E_0 \simeq 0.84$, at which the value of the entropy is close to $\ln 3$, meaning that the orbital degeneracy is lifted below this transition temperature. The inset of Fig. 4(c) shows a magnified picture of the entropy near T_{c2} , indicating the first-order transition. The specific heat $\mathcal{C} = \partial \mathcal{U} / \partial T$ is also shown in Fig. 4(d). There are two discontinuities corresponding to the spin and orbital orders.

Next we show in Fig. 5 the inverse of the diagonal susceptibilities $\chi_u^{\eta\mu;\eta\mu}$ (uniform) and $\chi_s^{\eta\mu;\eta\mu}$ (staggered) which are defined in Eqs. (32) and (33). First, we observe that the susceptibilities shown here are all positive, indicating a stable solution. The AF- S susceptibility of x, y, z type diverges at $T/E_0 \simeq 2.3$ signaling the onset of the antiferromagnetic order. Below this transition temperature, the longitudinal z component is decreased, while the perpendicular x, y components remain divergent. This behavior indicates the presence of the Goldstone mode, where the excitations are induced by rotating the z component into the xy plane, as in the standard Heisenberg model. Inside this magnetic phase, the orbital (F- Q) and spin-orbital (AF- T) susceptibilities, which are z^2 type in the orbital part, continue to grow and tend to diverge at a lower transition point (T_{c2}). As shown in Fig. 5(a), the “perpendicular” components, i.e., F- Q^{yz} and F- Q^{zx} , remain divergent below T_{c2} , indicating the presence of the Goldstone mode even for the orbital order in the spherical model. Namely, because of the symmetry of the spin-orbital space, energetically equivalent solutions exist and are obtained by rotating the order parameters.

Next we discuss the ground-state wave function, which includes the information of the order parameter at the zero-temperature limit. As is evident from the zero entropy at $T = 0$, we have a nondegenerate ground state. In the present

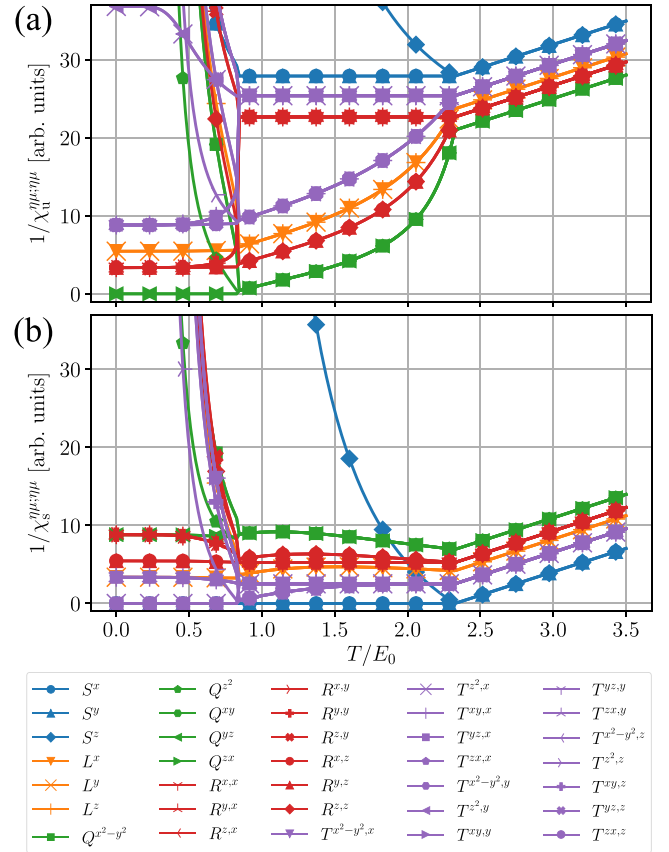


FIG. 5. Temperature dependence of the inverse of the (a) uniform and (b) staggered components of the diagonal susceptibilities. The energy unit is $E_0 = t^2/U$.

case, the ground-state wave function is very simple and is given using Eq. (4) by

$$|\psi_A\rangle = |n = 1, z, \downarrow\rangle_A, \quad (54)$$

$$|\psi_B\rangle = |n = 1, z, \uparrow\rangle_B \quad (55)$$

for each sublattice. This corresponds to the staggered spin ordered and uniform orbital ordered state, as is consistent with Fig. 4(a). More specifically, we can construct the order parameters from the direct product of the wave functions. In the present case, we obtain, at sublattice α ,

$$|\psi_\alpha\rangle\langle\psi_\alpha| = \mp \frac{1}{\sqrt{6}} S_\alpha^z - \frac{1}{\sqrt{3}} Q_\alpha^{z^2} \pm \frac{1}{\sqrt{3}} T_\alpha^{z^2, z} + \frac{1}{6}, \quad (56)$$

where the operators are defined in Eqs. (40)–(44). The upper (lower) sign is chosen for $\alpha = A$ ($\alpha = B$). The quantities that appear on the right-hand side are identical to the order parameters shown in Fig. 4(a).

3. Mean-field solutions for ferromagnetic Hund's coupling ($J > 0$)

We show the results for the $J/U = 0.1$ case, where the model is now relevant to materials with d electrons, to contrast with behaviors of the systems with antiferromagnetic Hund's coupling. Figure 6(a) shows the temperature evolution of the order parameters. As seen in Fig. 3, the largest coupling con-

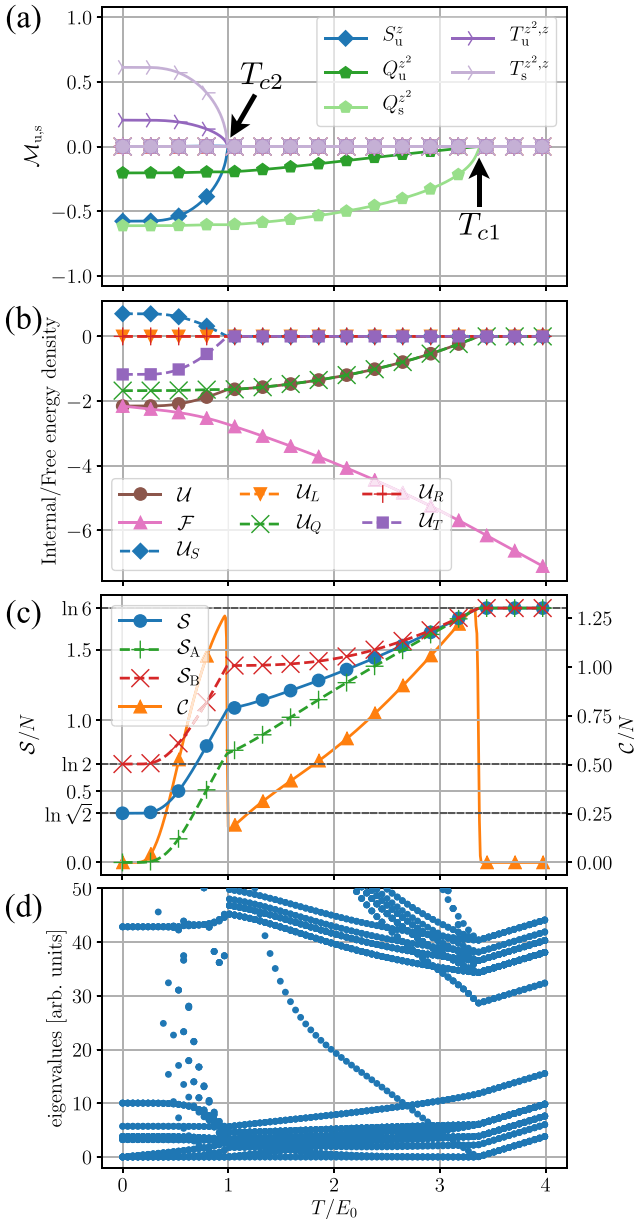


FIG. 6. Temperature dependence of (a) the order parameter, (b) the decomposed internal energy and total free energy density, (c) the single-site entropy (left axis) and the specific heat (right axis), and (d) the eigenvalues of the Hessian matrix \hat{a} calculated from Eq. (36) for the bipartite spherical model with $n = 1$, $J/U = 0.1$.

stant is $|I_Q|$ which is antiferromagnetic ($I_Q < 0$), and therefore the AF- Q order of z^2 type appears at the highest transition temperature (T_{c1}). The F- Q order of the same z^2 type is simultaneously induced. The rise of the order parameters near the transition temperature behaves as $\sim \sqrt{T_{c1} - T}$ for AF- Q and $\sim (T_{c1} - T)$ for F- Q . Hence the AF- Q is the primary order. From the symmetry argument, it can be shown that the F- Q order arises from AF- Q order since the coupling term in the Landau free energy has the form $Q_u^{z^2} (Q_s^{z^2})^2$. The existence of such a third-order term can be understood if one considers the symmetry in the plane of $Q^{z^2} - Q^{x^2-y^2}$ [26]. At lower temperatures, the magnetic F- S order appears, where T moments

of $T^{z^2,z}$ type are also finite. From the internal-energy analysis shown in Fig. 6(b), the relevant ordering at T_{c2} is induced from the interaction I_T while I_S is energetically unfavorable. Thus, comparing with the $J/U = -0.1$ case, the roles of magnetic order and electric (orbital) order are switched. This switching of the magnetic and orbital ordered states depending on the sign of J has also been reported in the two-orbital model [25].

We next show the temperature dependence of the entropy and specific heat in Fig. 6(c), where we have defined the sublattice-dependent entropy (Shannon entropy) by

$$S_\alpha = - \sum_n p_n^\alpha \ln p_n^\alpha, \quad (57)$$

where p_n^α is the probability for the n th state as calculated from the local partition function $Z_\alpha = \sum_n \exp(-\beta E_n^\alpha) = \sum_n p_n^\alpha Z_\alpha$. Since the entropy at zero temperature is zero at the A sublattice and is finite at the B sublattice, the two sublattices are inequivalent and are not simply connected by symmetry operations. This is due to the presence of both uniform and staggered orbital order parameters in Fig. 6(a). Indeed, the wave function in the ground state is written for each sublattice as

$$|\psi_A\rangle = |n = 1, z, \downarrow\rangle_A, \quad (58)$$

$$|\vec{\psi}_B\rangle = \begin{pmatrix} |n = 1, x, \downarrow\rangle_B \\ |n = 1, y, \downarrow\rangle_B \end{pmatrix}. \quad (59)$$

The remaining degeneracy at the B sublattice is because the x and y orbital components are equivalent. Namely, the triply degenerate state at each sublattice splits depending on the sublattice: The z orbital becomes energetically higher at the A sublattice and lower at the B sublattice. Thus the antiferromagnetic order of this type cannot lift the degeneracy completely.

Usually, the degeneracy is lifted by the interaction effects, and a unique ground state is expected. Then, one may suspect that the remaining degeneracy might indicate the instability of the solutions. In order to show that our degenerate ground states are really stable, we show the energy spectra of the Hessian matrix discussed in Sec. II C. As shown in Fig. 6(d), the excitation energies in terms of Landau theory are all positive or zero, and the system is thus stable. The degeneracy at $T = 0$ is due to the absence of the relevant interactions and will be resolved once the other types of interaction are included in more realistic situations.

We comment on the case where we allow only for uniform solutions, by having the geometrical frustration effect in mind, which does not favor simple staggered orders. Actually, the $n = 1$ uniform spherical model around $J = 0$ has no solution at any temperature because all of the coupling constants are negative (antiferromagnetic) in the spherical model (see Fig. 3). On the other hand, for a relatively large $|J|$ region the uniform solutions can exist. However, since the typical value of Hund's coupling is $|J|/U \sim 0.1$ or less, we do not enter the regime with larger $|J|$ in this paper.

C. $n = 3$ model

Here, we consider the model with three electrons per molecule and with antiferromagnetic Hund's coupling ($J <$

0). This model is more relevant to the existing fullerenes with half-filled t_{1u} molecular orbitals.

1. Coupling constants

We show the coefficients A [A being defined by Eq. (45)] in Table II. Since we consider the half-filled model, the initial and intermediate states for the two-site problem at the sites i and j relevant to I_{ij} are $(n_i, n_j) = (3, 3)$ and $(n_i, n_j) = (2, 4)$, respectively. Here, $n_i = 2$ and $n_i = 4$ states are connected with each other by the particle-hole (PH) transformation. The explicit form for the $n_i = 2$ state is the same as those given in Sec. III B, and thereby the $n = 4$ state can also be constructed from $n = 2$ accordingly. Below, we list the types of the intermediate states and their energies, specifically focusing on the $n_j = 4$ state.

The intermediate states with the excited energy $\Delta E_n = U - 8J$ are nine kinds of interorbital spin triplet state for $n_i = 2$ and the PH-transformed states for $n_j = 4$ such as $b_{j,z}^\dagger c_{j,y,\uparrow}^\dagger c_{j,x,\uparrow}^\dagger |0\rangle$. For $\Delta E_n = U - 6J$, the intermediate states are the interorbital spin triplet states for $n_i = 2$ and the PH-transformed states which have interorbital spin singlet states such as $\frac{1}{\sqrt{2}} b_{j,z}^\dagger (c_{j,y,\downarrow}^\dagger c_{j,x,\uparrow}^\dagger - c_{j,y,\uparrow}^\dagger c_{j,x,\downarrow}^\dagger) |0\rangle$ or intraorbital spin singlet with antibonding states such as $\frac{\sqrt{2}}{3} (2b_{j,z}^\dagger b_{j,y}^\dagger - b_{j,z}^\dagger b_{j,x}^\dagger - b_{j,y}^\dagger b_{j,x}^\dagger) |0\rangle$. For $\Delta E_n = U - 4J$, the intermediate states are the interorbital spin singlet or intraorbital spin singlet with antibonding states for $n_i = 2$ and their PH-transformed versions for the j site. For $\Delta E_n = U - 3J$, the intermediate states are the intraorbital spin singlet and bonding states for $n_i = 2$ and the states which have an interorbital spin triplet for $n_j = 4$. For $\Delta E_n = U - J$, the intermediate states are the interorbital spin singlet or intraorbital spin singlet with antibonding states ($n_i = 2$) and the intraorbital spin singlet and bonding state such as $\frac{1}{\sqrt{3}} (b_{j,z}^\dagger b_{j,y}^\dagger + b_{j,z}^\dagger b_{j,x}^\dagger + b_{j,y}^\dagger b_{j,x}^\dagger) |0\rangle$ for $n_j = 4$. Finally, for $\Delta E_n = U + 2J$, which is the lowest among the excited states for $J < 0$, the intermediate state is nondegenerate and is written as the intraorbital spin singlet with bonding state for $n_i = 2$ and its PH-transformed states for $n_j = 4$. In Table II, we also summarize the number of the degeneracy for each ΔE_n as in Table I.

Figure 7 shows the Hund's coupling dependence of the coupling constants. The perturbation theory is justified for $-1/2 < J/U < 0$ where any level cross for the unperturbed

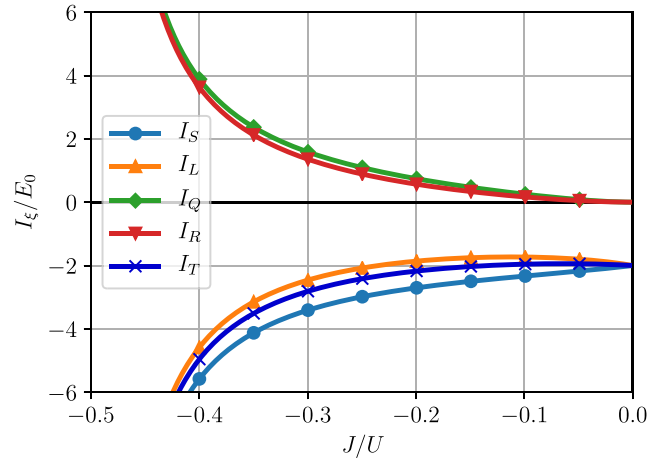


FIG. 7. Hund's coupling ratio J/U dependence of the coupling constants for the $n = 3$ spherical model.

Hamiltonian does not occur. If we consider $J > 0$, the ground state is a total spin $S = 3/2$ state (e.g., $c_{i,z,\uparrow}^\dagger c_{i,y,\uparrow}^\dagger c_{i,x,\uparrow}^\dagger |0\rangle_i$) and is different from $J < 0$ (see Fig. 2). This point is in contrast with the $n = 1$ case, where the ground state of the local Hamiltonian is not dependent on the sign of J as shown in Fig. 3. It is notable that the coupling constants for $n = 3$ case are similar to those of the $n = 1$ spherical model in the region near $J/U = -0.5$, where the same physical behavior is expected.

2. Mean-field solutions for the bipartite lattice

We show in Fig. 8(a) the order parameters for the bipartite lattice model with $n = 3$ and $J/U = -0.1$. At $T_{c1} \simeq 2.3E_0$, the system shows antiferromagnetic order, which is consistent with the largest coupling constant shown in Fig. 7. With decreasing temperature, the second-order transition at T_{c2} appears, where the $F-Q^{z^2}$ and $AF-T^{z^2,z}$ order parameters are additionally induced. We emphasize that this orbital order is not of the ordinary orbital moment of electrons, but of the doublons relevant to the antiferromagnetic Hund's coupling as discussed in Sec. II A.

Figure 8(b) shows the temperature dependences of the internal energies and free energy. We show the order-parameter-resolved energies, and all the components decrease

TABLE II. Coefficients A in Eq. (45) for the $n = 3$ spherical model. The ground state is written as $|\gamma_i, \sigma_i\rangle_i |\gamma_j, \sigma_j\rangle_j$, and its energy is $2(3U - 4J)$. We add the details for the intermediate state in the main text. We also show the number of the degeneracy for each energy level of the intermediate two-site state.

	ΔE_n					
	$U - 8J$	$U - 6J$	$U - 4J$	$U - 3J$	$U - J$	$U + 2J$
Degeneracy	162	180	50	36	20	2
$\xi = S$	1/2	-5/3	25/18	-4/3	20/9	8/9
$\xi = L$	9/8	-5/4	25/72	2	-10/9	8/9
$\xi = Q$	-9/8	1/4	-1/72	2	-2/9	-8/9
$\xi = R$	-1/8	-5/12	-25/72	2/3	10/9	-8/9
$\xi = T$	1/8	1/12	1/72	2/3	2/9	8/9
$\xi = 0$	-9/2	-5	-25/18	-4	-20/9	-8/9

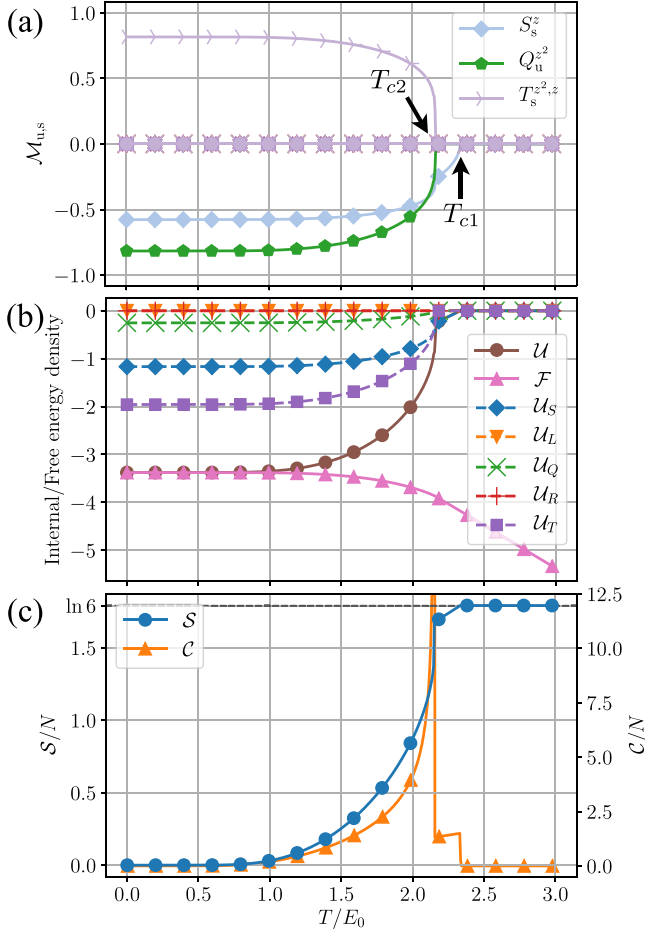


FIG. 8. Temperature dependence of (a) the order parameter, (b) the decomposed internal energy and total free energy density, and (c) the entropy (left axis) and the specific heat (right axis) for the $n = 3$ bipartite spherical model with $J/U = -0.1$. The horizontal axis is normalized by $E_0 = t^2/U$.

upon entering the ordered phase. While this is in contrast to the $n = 1$ cases shown in the previous sections, the largest energy gain arises from the AF- T order.

We show in Fig. 8(c) the entropy and specific heat. The clear jump in the specific heat at T_{c1} indicates the second-order phase transition, and the jump in the entropy at T_{c2} is the fingerprint of the first-order phase transition. The wave function in the ground state is

$$|\psi_A\rangle = |z, \downarrow\rangle_A, \quad (60)$$

$$|\psi_B\rangle = |z, \uparrow\rangle_B. \quad (61)$$

The ground state is thus nondegenerate as is consistent with the zero entropy at $T = 0$.

3. Single-sublattice solution

Having the geometrically frustrated lattice in mind, we assume that the spatially modulated solutions are not realized. Then we seek for the spatially uniform solutions (single sublattice) only.

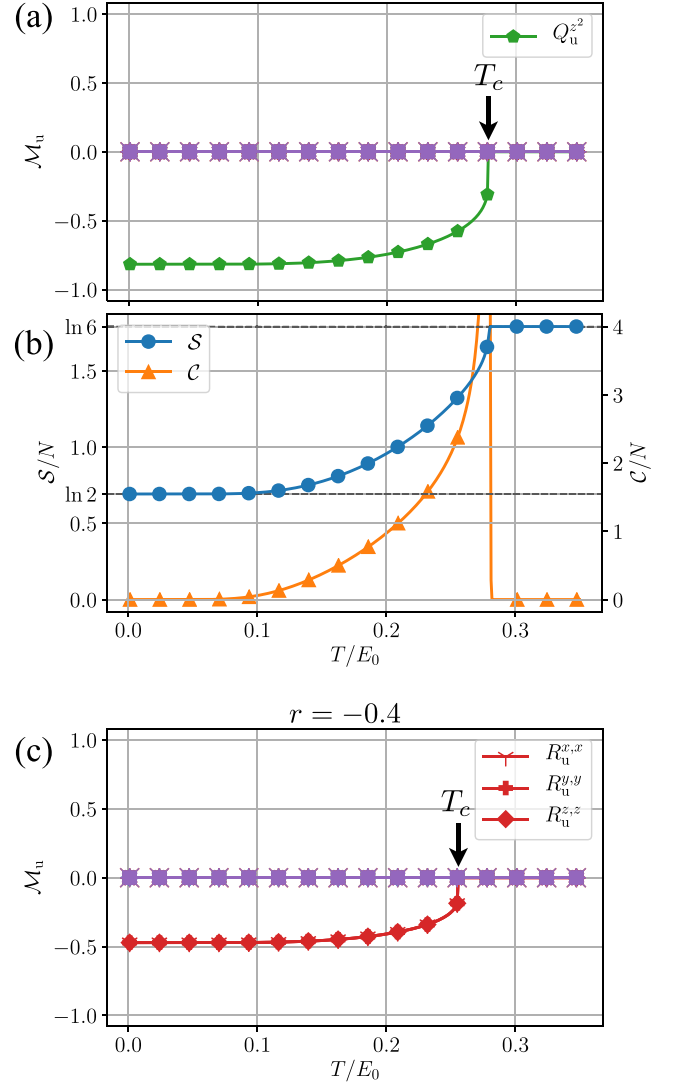


FIG. 9. Temperature dependence of (a) the order parameter and (b) the entropy (left axis) and the specific heat (right axis) for the $n = 3$ uniform spherical model with $J/U = -0.1$. (c) Similar order-parameter plots for the $n = 3$ single-sublattice model with coupling constant ratio $r = -0.4$. The energy unit is $E_0 = t^2/U$.

Figure 9(a) shows the order parameter for the single-sublattice model with $n = 3$, $J/U = -0.1$. The system shows the Q^{z^2} order at $T_c/E_0 \simeq 0.28$, which is consistent with the magnitude of the coupling constant shown in Fig. 7. The entropy and specific heat are shown in Fig. 9(b) with the left and right axis, respectively. The residual entropy $S = \ln 2$ remains, which is in accordance with the degeneracy of spin in the absence of the sublattice degrees of freedom. Namely, the wave function of the ground state is degenerated and is written as

$$|\vec{\psi}\rangle = \begin{pmatrix} |z, \uparrow\rangle \\ |z, \downarrow\rangle \end{pmatrix}. \quad (62)$$

We have confirmed that the eigenvalues of \hat{a} in Eq. (36) are all non-negative (not shown) and thus the ordered state is stable.

We also point out other interesting possibilities. The above orbital order is induced by the coupling constant $I_Q > 0$ in

Fig. 7. In this figure, it is notable that the values of I_Q and I_R are very close to each other. Then we try to search for other solutions by introducing the modified coupling constants defined as

$$\tilde{I}_Q = (1 + r)I_Q, \quad (63)$$

$$\tilde{I}_R = (1 - r)I_R, \quad (64)$$

where the original spherical model corresponds to $r = 0$.

We show the order parameters for the $n = 3$, $J/U = -0.1$ uniform model with the coupling constant ratio $r = -0.4$ in Fig. 9(c). Since the magnitude of the modified coupling constants satisfies $\tilde{I}_R > \tilde{I}_Q$ in the present condition, we obtain the solution for $R^{\mu,\mu}$ moments. Recalling the definition of the R moment, we may rewrite the order parameter as $R^{\mu,\mu} \sim L^\mu S^\mu$ symbolically. Therefore it is interpreted that the system has the effective spin-orbit coupling spontaneously. The wave function is written as

$$|\tilde{\psi}\rangle = \frac{1}{\sqrt{3}} \begin{pmatrix} |x, \uparrow\rangle - i|y, \uparrow\rangle - |z, \downarrow\rangle \\ -|x, \downarrow\rangle - i|y, \downarrow\rangle - |z, \uparrow\rangle \end{pmatrix}, \quad (65)$$

which indicates that the ground state is entangled with respect to spin and orbital. These doubly degenerate ground states are connected with each other by the time-reversal symmetry.

This “spontaneous spin-orbit coupling” splits the sixfold degeneracy into twofold and fourfold multiplets, and which is realized in the ground state is dependent on the sign of the order parameters. Our solutions show that the ground state is always doubly degenerate, and this should be related to the minimization of the entropy at low temperatures.

Thus, although the system at the original parameter shows the doublon-orbital ordering (Q), the system is located near the parameter range where the intriguing R order occurs. As discussed in Sec. II A the original spin-orbit coupling Λ_{SO} is tiny, but it might enter through the R -type ordering. Such a situation is realized only for the $n = 3$ model with the antiferromagnetic Hund’s coupling.

IV. NUMERICAL RESULTS FOR FULLERIDES

We show the numerical results for the fulleride in the strong-coupling regime by using the hopping parameters obtained by the first-principles calculation [40]. We take the intraorbital Coulomb interaction $U = 1$ eV and the Hund’s coupling $J/U = -0.1$ in the following.

A. A15 structure

First of all, we show in Fig. 10(a) the temperature dependence of order parameters for the strong-coupling-limit model of the realistic fulleride material with the A15 structure. The hopping parameters for Cs_3C_{60} are chosen $\{\text{A15-Cs}(V_{SC}^{\text{opt-P}})\}$ in Ref. [40]. The lattice structure is a bipartite lattice, and A and B sublattices are connected with each other by screw transformation (i.e., translation plus fourfold rotation). As shown in Fig. 10(a), at $T_{c1} \simeq 80$ K, the antiferromagnetic moment (AF- S) appears by the second-order phase transition. At lower temperatures, we identify the two successive phase transitions ($T_{c2,3}$) with orbital moment Q and spin-orbital moment T . These two Q , T moments share the same symmetry in the

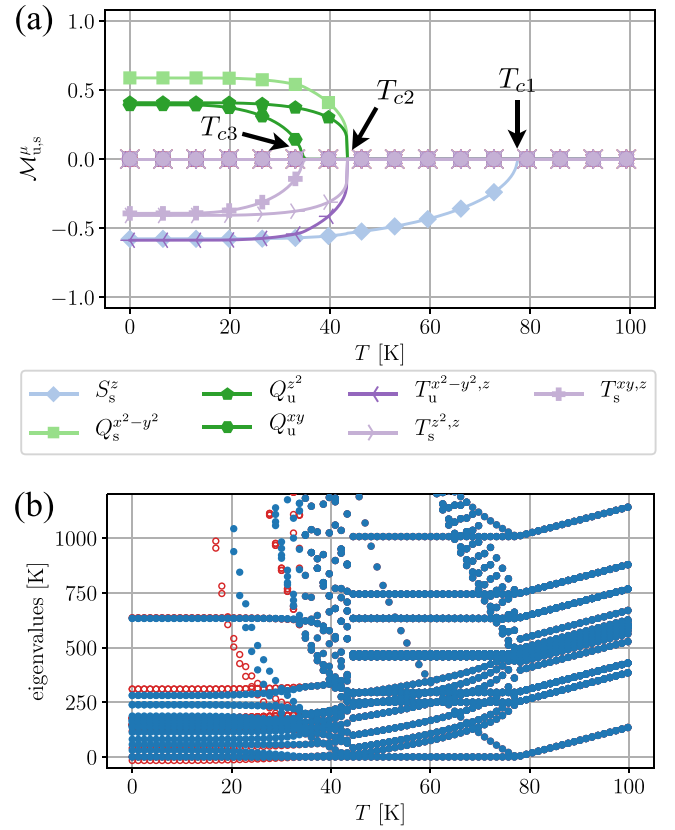


FIG. 10. Temperature dependence of (a) the order parameter and (b) the eigenvalues of the matrix \hat{a} calculated from Eq. (36) for the A15-fulleride model. The solid blue circles in (b) correspond to the solution given in (a). The open red circles in (b) represent the solution without the phase transition at T_{c3} .

presence of AF- S^z order. We cannot simply conclude which one is the primary order parameter, because the interaction has a complicated form for the realistic model and cannot be decomposed into each contribution as in the spherical model. We also note that our choice of parameter is not fine-tuned to reproduce correctly the transition temperature in the actual materials, although our results can be compared with the experiments semiquantitatively.

We show in Fig. 10(b) the eigenvalues (solid blue circles) of the Hessian matrix defined in Eq. (36). All the values are non-negative, and therefore the system is stable. On the other hand, we can also calculate the low-temperature solutions by suppressing the ordering at T_{c3} . The results are plotted as the open red circles in Fig. 10(b). In this case, the eigenvalues become partially negative, and hence the system is not stable although the entropy goes to zero even in this case. Thus the emergence of the order at T_{c3} is essential in order to reach the stable ground state.

We discuss the origin of the second orbital order at T_{c3} in more detail. Below, we concentrate on the properties of Q moments to make the discussion simple, since the symmetry of Q is the same as that of T below the transition temperature T_{c1} . Figure 11(a) shows the orbital order parameters for sublattice A (left panel) and B (right panel) slightly below the transition temperature T_{c2} (but above T_{c3}). The three patterns

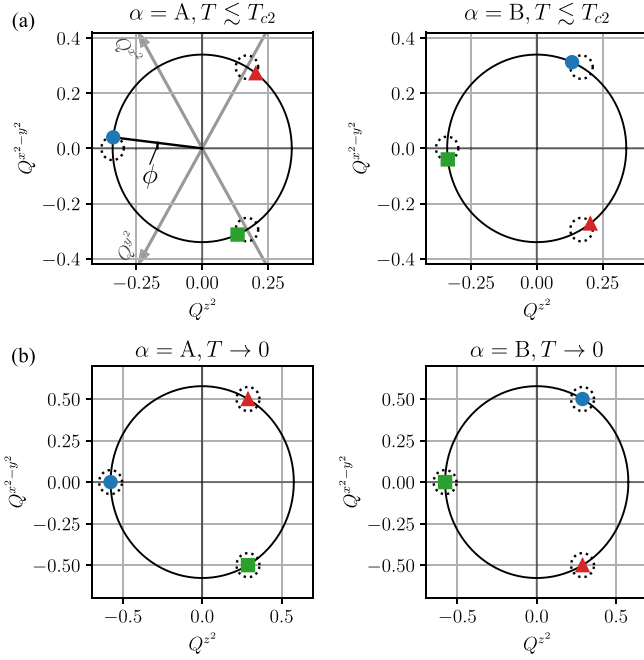


FIG. 11. (a) Sublattice-dependent order parameters in the plane of $Q^z{}^2$ - $Q^{x^2-y^2}$ for A (left) and B (right) sublattices at $T = 40.4$ K ($< T_{c2}$). (b) Similar plots at the low-temperature limit *without* the transition at T_{c3} . The dashed circles in (a) and (b) correspond to the solutions in the system with fourfold symmetries. Each color shows a different kind of solution, all of which share the same free energy. The gray arrows with Q^{x^2} or Q^{y^2} are the guide for taking the other quantization axis. Specifically, the solution given in Fig. 10(a) corresponds to the red triangles in (a). The angle ϕ in the left panel of (a) is the deviation from the horizontal axis.

are obtained depending on the initial condition and hence are degenerate solutions. It is seen from Fig. 11(a) that the plane of $X_\alpha = Q_\alpha^z{}^2$ and $Y_\alpha = Q_\alpha^{x^2-y^2}$ has a threefold rotational symmetry and the equilateral-triangle points, where the free energy minima are located, are tilted from the X axis. This tilt angle remains finite at low temperatures below T_{c3} .

This result can be understood from the Landau theory: We can show that, without fourfold rotational symmetry as in T_h point-group symmetry in fulleride materials, the Landau free energy is written in the restricted order-parameter space as

$$\mathcal{F}_L = \sum_{\alpha=A,B} [c_1 X_\alpha (X_\alpha^2 - 3Y_\alpha^2) + c_2 s_\alpha Y_\alpha (3X_\alpha^2 - Y_\alpha^2)], \quad (66)$$

where $s_{\alpha=A} = +1$ and $s_{\alpha=B} = -1$. We have considered only the third-order term for our purpose. This is consistent with the numerical results, and the tilt of the angle is due to the presence of c_2 term. The tilt angle is estimated with the polar coordinates $X = r \cos \theta$ and $Y = r \sin \theta$, leading to another expression of the free energy $\mathcal{F}_L \propto \cos(3\theta + \phi)$, with $\phi = \tan^{-1} c_2/c_1$ being the tilt angle. For example, one can estimate this angle from Fig. 11(a) as $\phi = 6.76^\circ$. The A15 structure has screw symmetry, i.e., the combination of the translation along [111] and fourfold rotation around the x, y, z axes, which relates the order parameters at the A and B sublattices. Indeed,

TABLE III. Remaining symmetries in several temperature regimes. Θ , $C_4^{x,y,z}$, T , and C_3 represent the time-reversal, fourfold rotation, partial translation, and threefold rotation operations, respectively. This table originates from the solution with red triangles shown in Fig. 10(a). N/A, not applicable.

Temperature	Remaining symmetries
$T_{c1} < T$	$\Theta, C_4^{x,y,z} \times T, C_3$
$T_{c2} < T < T_{c1}$	$C_4^{x,y,z} \times T, C_3$
$T_{c3} < T < T_{c2}$	$C_4^z \times T$
$T < T_{c3}$	N/A

the above Landau free energy is invariant under the threefold rotation and screw transformations.

If the fourfold symmetry is present, the condition $c_2 = 0$ or $\phi = 0$ is required. In Fig. 11(b), we show the order parameters at $T \rightarrow 0$ *without* the second orbital ordering below T_{c3} , where the fourfold symmetry seems to be effectively recovered since the tilt angle goes to zero when $T \rightarrow 0$. Hence the origin of the second orbital order in Fig. 10(a) below T_{c3} is interpreted as being induced from this emergent symmetry at low temperatures which provides an additional free energy gain.

Let us further discuss the orbital ordered state of the A15 fulleride from a symmetry point of view. First we summarize the symmetries in the disordered state at high temperatures. There are the time-reversal symmetry Θ and the three-fold rotational symmetry C_3 along the [111] direction. We also have the screw symmetry denoted by $C_4^{x,y,z} \times T$, where $C_4^{x,y,z}$ is the fourfold rotation around the x, y, z axes and T is the partial translation that exchanges A and B sublattices of the A15 lattice. We note that $C_4^{x,y,z}$ and T themselves are not a symmetry operation of fullerenes.

Below T_{c1} , the system spontaneously breaks the time-reversal symmetry due to the spin ordering. In the intermediate temperatures $T_{c3} < T < T_{c2}$, the doublon's orbital ordered state with $Q^z{}^2$ and $Q^{x^2-y^2}$ breaks the threefold rotational symmetry C_3 and some of the screw symmetries spontaneously. Notably, there is a still-remaining screw symmetry which can be seen from, e.g., the red triangles of Fig. 11(a): The transformation $C_4^z \times T$ keeps the orbital ordered system invariant. This remaining symmetry causes another phase transition at T_{c3} , where the order parameter Q^{xy} appears and breaks the remaining screw symmetry. We summarize the above relations between the temperature range and the remaining symmetries in Table III.

B. fcc structure

Finally, we consider the fulleride material with the fcc structure. The spin-orbital model in the strong-coupling limit is obtained by using the hopping parameters for Rb_3C_{60} in Ref. [40]. Because of the geometrically frustrated nature of the fcc lattice, we here seek for only the spatially uniform ordered states.

Figure 12(a) shows the temperature evolution of the order parameters. Here, the primary order parameter is the uniform L^z moment, which breaks the time-reversal symmetry.

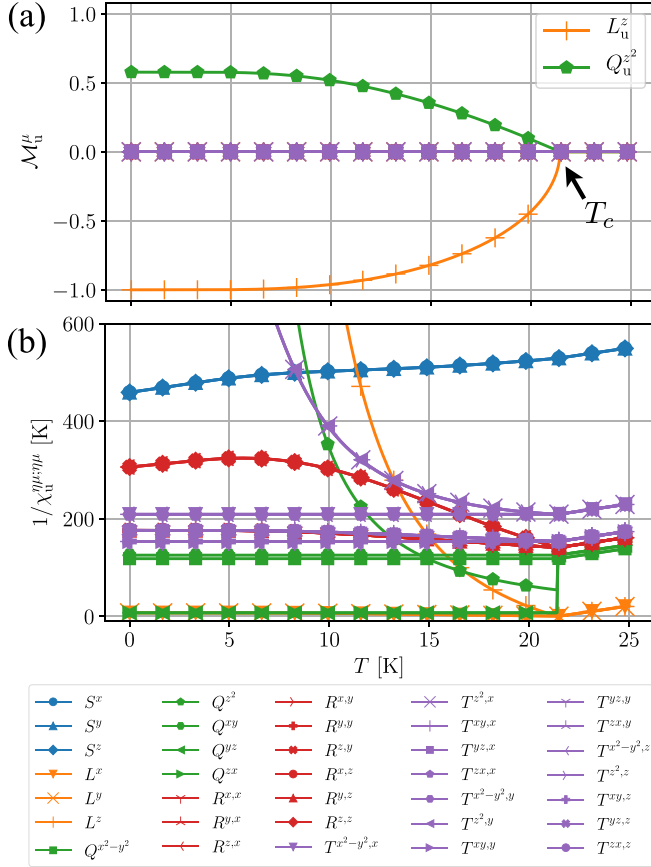


FIG. 12. Temperature dependence of (a) the order parameter and (b) the inverse of the diagonal susceptibility for the uniform fcc fulleride model with $J/U = -0.1$.

The L^z order arises as $(T_c - T)^{1/2}$, and the Q^{z^2} order is also induced simultaneously with the linear temperature dependence $\propto (T_c - T)$. The latter Q moment is induced from the coupling term with the form $(L^z)^2 Q^{z^2}$ in the Landau free energy. We note that L_z is not induced when Q^{z^2} is a primary order parameter from that coupling, since L_z and Q^{z^2} have different time-reversal symmetry [$(L^z)^2$ and Q^{z^2} are the same]. The ground-state wave function is written in a simple form as

$$|\tilde{\psi}\rangle = \frac{1}{\sqrt{2}} \left(|x, \uparrow\rangle - i|y, \uparrow\rangle \right), \quad (67)$$

where the complex wave function clearly shows the time-reversal symmetry breaking. We note that this orbital moment is not a simple orbital motion around the fullerene molecule, but a complex motion of the three-electron state given in Eq. (4). In our calculations the spin S order does not occur, and the ground state is doubly degenerate at each site. The stability of the solution is checked by the non-negative eigenvalues of the Hessian matrix.

The results found here are different from the spherical case discussed in Sec. III C 3. The difference is due to the specific form of the tight-binding hopping parameters. We show one of the coupling constants I_L for the nearest-neighbor

sites as

$$\begin{pmatrix} I_1 & I_2 & 0 \\ I_2 & -I_3 & 0 \\ 0 & 0 & I_4 \end{pmatrix}, \quad \mathbf{R} = \left(\frac{a}{2}, \frac{a}{2}, 0 \right), \quad (68)$$

where \mathbf{R} is the direction of the NN molecules and a is the lattice constant for the fcc fulleride. The information for the other NN pairs is constructed from the symmetry operations. The values of the matrix element are $I_1 = 12.5$, $I_2 = 9.77$, $I_3 = 0.511$, and $I_4 = 20.1$ in units of K in the present models. The coupling constant has the same symmetry as the hopping parameters in Ref. [40] as required by the space-group symmetry. The nearest-neighbor coupling constant is largest and is positive, which favors the uniform magnetic orbital moment \mathbf{L} . As for the next-nearest-neighbor site, the coupling constant matrices are diagonal, and every component of them is smaller than the nearest-neighbor ones.

Since the spin S moment has the same symmetry as \mathbf{L} , it can in general be simultaneously induced under the small but finite spin-orbit coupling. However, as discussed in Sec. II A, the magnitude of the effective spin-orbit coupling for the doublon orbital is $\Delta_{\text{SO}} \sim 10^{-9}$ eV, which can be regarded as zero in practice. Hence the spin order can occur independently at low temperatures. The absence of the spin S order is interpreted from the point of view of the coupling constant. Figure 12(b) shows the temperature dependence of the inverse of the diagonal susceptibilities. The blue lines represent the magnetic susceptibility (S), which indicates that the coupling constants of S are antiferromagnetic owing to the negative Curie-Weiss temperature. In this case, the transition temperature should be very low due to the geometrical frustration of the fcc lattice, but finally the system should show some magnetic ordering [41].

C. Discussion

The models in this section are based on band structure calculation results. Furthermore, the fulleride materials can be located in the Mott insulator regime depending on the pressure. Hence our results are potentially applicable to real materials. In fulleride materials, antiferromagnetic orders have been experimentally identified at low temperatures, while orbital orders have not yet been reported. Based on our results, we propose that at low temperatures the orbital ordered moments \mathbf{Q} are induced with two successive transitions for A15 structures, and \mathbf{L} moments may appear for fcc structures. Such fingerprints of the orbital orders may be found in thermodynamic quantities in principle. Here, the orbital moment is not for a usual electron but for the doublons specific to the systems with antiferromagnetic Hund's coupling as emphasized in this paper. On the other hand, since the real compounds are polycrystals and disorder effects are also present, the orbital orders might be smeared out in realistic situations. In this context, the effect of disorders on our spin-orbital model is an interesting issue for future research which would make comparing the theoretical results with experimental observations more direct. Moreover, the antiferromagnetic Hund's coupling originates from the electron-phonon coupling. The resultant retardation effects

are also not included in this paper and are an important issue for more realistic arguments.

V. SUMMARY AND OUTLOOK

In order to clarify the properties of strongly correlated electrons in fulleride superconductors, we have constructed the spin-orbital model in the strong-coupling limit. We begin with the three-orbital Hubbard model with antiferromagnetic Hund's coupling which is realized by the coupling between the electronic degrees of freedom and anisotropic Jahn-Teller molecular vibrations. In this case, the pair hopping effect among the different orbitals becomes relevant in strong contrast to the multiorbital d -electron systems with ferromagnetic Hund's coupling. We have mainly considered the half-filled $n = 3$ case relevant to real materials, where it is composed of singly occupied (singlon) plus doubly occupied (doublon) orbitals as illustrated in Fig. 1. The correlated ground state for an isolated fullerene molecule is sixfold degenerate and is characterized by the spin and orbital indices. This is a situation similar to the $n = 1$ ground states, and the analogy between $n = 3$ and $n = 1$ helps us in interpreting the results. The usual orbital moment, which is present for the $n = 1$ case, is absent for $n = 3$ because of the correlated nature of the wave function, and instead the active orbital moment characteristic for doublons exists. As a result, the spin-orbit coupling, which is of the order of 1 meV for p electrons, becomes 1 neV because of the extended nature of the molecular orbitals and the correlation effects.

We have applied the second-order perturbation theory with respect to the intermolecule hopping and have obtained the localized spin-orbital model specific to the fullerenes. The obtained spin-orbital model is analyzed by employing the mean-field approximation. For reference, we have first solved the spherical $n = 1$ model for both ferromagnetic and antiferromagnetic Hund's couplings with a spherical limit for the bipartite lattice. We then applied our method to the $n = 3$ model, where the magnetic order is found at relatively high temperatures and the orbital order also occurs at lower temperatures. The temperature dependences of the physical quantities, such as order parameters, internal and free energies, specific heat, entropy, and susceptibilities, are investigated in detail. The thermodynamic stability is also studied

based on the Hessian matrix derived from the inverse susceptibilities and is checked by confirming that all the eigenvalues are non-negative.

We have also considered the realistic situation in alkali-doped fullerenes, by using the tight-binding parameters derived from first-principles calculations. For the choice of the lattice structure, we have taken both the bipartite A15 and fcc structures, whose hopping parameters have been derived in Ref. [40]. For the A15 structure, the antiferromagnetic order occurs at high temperatures, and the electric orbital orders arise at lower temperatures with two successive transitions. The first orbital order is already captured in the spherical model, but the second orbital order is characteristic for the T_h symmetry in fullerene materials where only the threefold rotation symmetry exists. This point has been discussed in detail based on the Landau theory and symmetries. For the fcc model, we have concentrated on the spatially uniform solutions due to the geometrically frustrated nature of the lattice. We have found that the magnetic orbital order occurs. Although this orbital moment has the same symmetry as the electronic spin, the spin moment is not induced simultaneously in fullerene since the spin-orbit coupling is tiny as mentioned above. Thus the spin moment can order independently and is expected to be antiferromagnetically ordered in the ground state, where the transition temperature is expected to be low owing to the geometrical frustration of the fcc lattice.

Our formalism itself is constructed in a very general way and can be applied to any systems in the strong-coupling limit with integer fillings per atom or molecule. In this context, it would be desirable to develop the general framework for the strong-coupling-limit spin-orbital model with the combination of the hopping parameters in the Wannier functions obtained from the band structure calculations. This application is of interest specifically in studying the ordered state of the multiorbital electronic systems including transition metals and organic materials. This point remains to be explored and is an intriguing issue for future research.

ACKNOWLEDGMENTS

This work was supported by JSPS KAKENHI Grants No. JP18K13490, No. JP19H01842, and No. JP21K03459.

-
- [1] A. F. Hebard, M. J. Rosseinsky, R. C. Haddon, D. W. Murphy, S. H. Glarum, T. T. M. Palstra, A. P. Ramirez, and A. R. Kortan, *Nature (London)* **350**, 600 (1991).
 - [2] M. J. Rosseinsky, A. P. Ramirez, S. H. Glarum, D. W. Murphy, R. C. Haddon, A. F. Hebard, T. T. M. Palstra, A. R. Kortan, S. M. Zahurak, and A. V. Makhija, *Phys. Rev. Lett.* **66**, 2830 (1991).
 - [3] K. Holczer, O. Klein, S.-m. Huang, R. B. Kaner, K.-j. Fu, R. L. Whetten, and F. Diederich, *Science* **252**, 1154 (1991).
 - [4] K. Tanigaki, T. W. Ebbesen, S. Saito, J. Mizuki, J. S. Tsai, Y. Kubo, and S. Kuroshima, *Nature (London)* **352**, 222 (1991).
 - [5] R. M. Fleming, A. P. Ramirez, M. J. Rosseinsky, D. W. Murphy, R. C. Haddon, S. M. Zahurak, and A. V. Makhija, *Nature (London)* **352**, 787 (1991).
 - [6] A. Y. Ganin, Y. Takabayashi, Y. Z. Khimyak, S. Margadonna, A. Tamai, M. J. Rosseinsky, and K. Prassides, *Nat. Mater.* **7**, 367 (2008).
 - [7] Y. Takabayashi, A. Y. Ganin, P. Jeglič, D. Arčon, T. Takano, Y. Iwasa, Y. Ohishi, M. Takata, N. Takeshita, K. Prassides, and M. J. Rosseinsky, *Science* **323**, 1585 (2009).
 - [8] A. Y. Ganin, Y. Takabayashi, P. Jeglič, D. Arčon, A. Potočník, P. J. Baker, Y. Ohishi, M. T. McDonald, M. D. Tzirakis, A. McLennan, G. R. Darling, M. Takata, M. J. Rosseinsky, and K. Prassides, *Nature (London)* **466**, 221 (2010).

- [9] O. Gunnarsson, *Rev. Mod. Phys.* **69**, 575 (1997).
- [10] M. Fabrizio and E. Tosatti, *Phys. Rev. B* **55**, 13465 (1997).
- [11] M. Capone, M. Fabrizio, C. Castellani, and E. Tosatti, *Science* **296**, 2364 (2002).
- [12] M. Capone, M. Fabrizio, C. Castellani, and E. Tosatti, *Rev. Mod. Phys.* **81**, 943 (2009).
- [13] Y. Nomura, S. Sakai, M. Capone, and R. Arita, *J. Phys.: Condens. Matter* **28**, 153001 (2016).
- [14] Y. Takabayashi and K. Prassides, *Philos. Trans. R. Soc., A* **374**, 20150320 (2016).
- [15] R. H. Zadik, Y. Takabayashi, G. Klupp, R. H. Colman, A. Y. Ganin, A. Potočník, P. Jeglič, D. Arčon, P. Matus, K. Kamarás, Y. Kasahara, Y. Iwasa, A. N. Fitch, Y. Ohishi, G. Garbarino, K. Kato, M. J. Rosseinsky, and K. Prassides, *Sci. Adv.* **1**, e1500059 (2015).
- [16] Y. Kasahara, Y. Takeuchi, R. H. Zadik, Y. Takabayashi, R. H. Colman, R. D. McDonald, M. J. Rosseinsky, K. Prassides, and Y. Iwasa, *Nat. Commun.* **8**, 14467 (2017).
- [17] S. Han, M.-X. Guan, C.-L. Song, Y.-L. Wang, M.-Q. Ren, S. Meng, X.-C. Ma, and Q.-K. Xue, *Phys. Rev. B* **101**, 085413 (2020).
- [18] M.-Q. Ren, S. Han, S.-Z. Wang, J.-Q. Fan, C.-L. Song, X.-C. Ma, and Q.-K. Xue, *Phys. Rev. Lett.* **124**, 187001 (2020).
- [19] M. Mitrano, A. Cantaluppi, D. Nicoletti, S. Kaiser, A. Perucchi, S. Lupi, P. D. Pietro, D. Pontiroli, M. Riccò, S. R. Clark, D. Jaksch, and A. Cavalleri, *Nature (London)* **530**, 461 (2016).
- [20] A. Cantaluppi, M. Buzzi, G. Jotzu, D. Nicoletti, M. Mitrano, D. Pontiroli, M. Riccò, A. Perucchi, P. D. Pietro, and A. Cavalleri, *Nat. Phys.* **14**, 837 (2018).
- [21] M. Capone, M. Fabrizio, P. Giannozzi, and E. Tosatti, *Phys. Rev. B* **62**, 7619 (2000).
- [22] Y. Nomura, S. Sakai, M. Capone, and R. Arita, *Sci. Adv.* **1**, e1500568 (2015).
- [23] A. Koga and P. Werner, *Phys. Rev. B* **91**, 085108 (2015).
- [24] S. Hoshino and P. Werner, *Phys. Rev. B* **93**, 155161 (2016).
- [25] K. Steiner, S. Hoshino, Y. Nomura, and P. Werner, *Phys. Rev. B* **94**, 075107 (2016).
- [26] S. Hoshino and P. Werner, *Phys. Rev. Lett.* **118**, 177002 (2017).
- [27] K. Ishigaki, J. Nasu, A. Koga, S. Hoshino, and P. Werner, *Phys. Rev. B* **98**, 235120 (2018).
- [28] K. Ishigaki, J. Nasu, A. Koga, S. Hoshino, and P. Werner, *Phys. Rev. B* **99**, 085131 (2019).
- [29] C. Yue, S. Hoshino, and P. Werner, *Phys. Rev. B* **102**, 195103 (2020).
- [30] S. Hoshino, P. Werner, and R. Arita, *Phys. Rev. B* **99**, 235133 (2019).
- [31] T. Misawa and M. Imada, *arXiv:1711.10205*.
- [32] K. I. Kugel and D. I. Khomskii, *Pis'ma Zh. Eksp. Teor. Fiz.* **15**, 629 (1972) [*JETP Lett.* **15**, 446 (1972)].
- [33] K. I. Kugel and D. I. Khomskii, *Zh. Eksp. Teor. Fiz.* **64**, 1429 (1973) [*Sov. Phys. JETP* **37**, 725 (1973)].
- [34] S. Inagaki, *J. Phys. Soc. Jpn.* **39**, 596 (1975).
- [35] S. Ishihara, J. Inoue, and S. Maekawa, *Phys. Rev. B* **55**, 8280 (1997).
- [36] L. F. Feiner and A. M. Oleś, *Phys. Rev. B* **59**, 3295 (1999).
- [37] B. Normand and A. M. Oleś, *Phys. Rev. B* **78**, 094427 (2008).
- [38] Y. Nomura and R. Arita, *Phys. Rev. B* **92**, 245108 (2015).
- [39] E. Tosatti, N. Manini, and O. Gunnarsson, *Phys. Rev. B* **54**, 17184 (1996).
- [40] Y. Nomura, K. Nakamura, and R. Arita, *Phys. Rev. B* **85**, 155452 (2012).
- [41] Y. Kasahara, Y. Takeuchi, T. Itou, R. H. Zadik, Y. Takabayashi, A. Y. Ganin, D. Arčon, M. J. Rosseinsky, K. Prassides, and Y. Iwasa, *Phys. Rev. B* **90**, 014413 (2014).